Gravitational form factors of the baryon octet with flavor SU(3) symmetry breaking

Ho-Yeon Won,[1,*] June-Young Kim,[1,2,†] and Hyun-Chul Kim[1,3,‡]

[1]*Department of Physics, Inha University, Incheon 402-751, South Korea*
[2]*Theory Center, Jefferson Lab, Newport News, Virginia 23606, USA*
[3]*School of Physics, Korea Institute for Advanced Study (KIAS), Seoul 02455, South Korea*

(Received 10 October 2022; accepted 25 November 2022; published 12 December 2022)

We investigate the gravitational form factors of the baryon octet within the framework of the SU(3) chiral quark-soliton model, considering the effects of flavor SU(3) symmetry breaking, and with the corresponding energy-momentum tensor distributions. We examine the effects of flavor SU(3) symmetry breaking to the mass, angular momentum, pressure, and shear force distributions of the baryon octet. We first find that a heavier baryon is energetically more compact than a lighter one. For the spin distributions of the baryon octet, they are properly normalized to their spins and are decomposed into the flavor-singlet axial charge and the orbital angular momentum even when the flavor SU(3) symmetry is broken. While the effects of the flavor SU(3) symmetry breaking differently contribute to the angular momentum distributions for the octet baryons, they are found to be rather small. The spin and orbital angular momentum almost equally contribute to the angular momentum distributions for the octet baryons. We also estimate the effects of the flavor SU(3) symmetry breaking to the pressure and shear force distributions. Interestingly, even if we include the effects of the SU(3) flavor symmetry breaking, then the shear force distributions are kept to be positive over r. It indicates that the Polyakov and Schweitzer local stability condition is kept to be intact with the flavor SU(3) symmetry broken. Lastly, we discuss how much the gravitational form factors vary with the effects of flavor SU(3) symmetry breaking considered.

DOI: 10.1103/PhysRevD.106.114009

I. INTRODUCTION

It is of great importance to understand the mechanical structure of a baryon as much as the electromagnetic (EM) one, since it reveals how the baryon is mechanically shaped by its partons. The gravitational form factors (GFFs) of a baryon provide information on its mechanical properties such as the mass, spin, pressure, and shear force. At an early stage, the GFFs were considered as a purely academic subject [1,2] due to the difficulty in having access to them experimentally. However, the generalized parton distributions (GPDs) have paved way for extracting the GFFs experimentally, since the EM form factors and GFFs are defined, respectively, as the first and second Mellin moments of the GPDs that can be measured by the hard exclusive process such as deeply virtual Compton scattering (DVCS) or hard exclusive meson production. Recently, the first measurement of the nucleon D-term form factors from DVCS was reported [3–5]. The transition GPDs will soon be extracted from the experimental data on the hard exclusive meson production $p \to \Delta^{++}\pi^-$ at Jefferson Lab [6,7]. This measurement will lead to the $N \to \Delta$ transition GFFs [8]. Moreover, the upcoming Electric-Ion Collider (EIC) project will unveil the fractions of the mass and spin of the nucleon, which are taken up by quarks and gluons inside it. It is well known that the quark content of the nucleon spin is small (see a recent review [9]) and the strange quark is polarized negatively ($\Delta s \sim -0.10$ [10]). This implies that the gluon spin and the orbital motion of the quarks and gluon should considerably contribute to the nucleon spin. The future EIC project will provide a clue to the spin structure of the nucleon.

The GFFs for spin-1/2 particles parametrize the matrix element of the energy-momentum tensor (EMT) current [1,2,11,12]. It was recently generalized to higher-spin particles [13] in a systematic way. Based on this parametrization, the GFFs of the nucleon have been intensively investigated in various approaches [14–42]. The parity flip transition [43–45] and $N \to \Delta$ transition [8] matrix elements of the EMT current were also parametrized. For a spin-1 particle, the model-independent formalism for the GFFs and

*hoywon@inha.edu
†Jun-Young.Kim@ruhr-uni-bochum.de
‡hchkim@inha.ac.kr

distributions were studied in Refs. [46–50] and the GFFs were obtained by many theoretical works [37,51–53]. The GFFs for a spin-3/2 particle were also examined [37,54–56]. On the other hand, the GFFs of the baryon octet were much less studied [57]. To compute them, we need to consider the flavor SU(3) symmetry and its breakdown. Since the effects of the flavor SU(3) symmetry breaking on the GFFs and related distributions have never been examined, it is worthwhile to investigate them. In particular, it is critical to check whether the local and global stability conditions are satisfied with the flavor SU(3) symmetry broken.

While the three-dimensional (3D) EMT distributions, which show how partons are spatially distributed inside a baryon in the Breit frame (BF) [58], were obtained by the 3D Fourier transform of the corresponding GFFs, there have been serious criticisms of the 3D distributions of the nucleon [59–63]. The 3D distributions depend on the shape of the wave packet of a baryon, and this wave packet cannot be localized below the Compton wavelength. It brings about ambiguous relativistic effects of which the contribution is approximated by around 20% for the nucleon. Thus, they cannot be neglected anymore. To circumvent these ambiguous relativistic effects, the two-dimensional (2D) spatial EMT distributions have been considered in the infinite momentum frame (IMF) or on the light front (LF). The ambiguous relativistic corrections are kinematically suppressed then [26,41,42]. However, we have to pay the price that we lose information in the longitudinal direction.

There is yet another way of understanding the 3D distributions by defining them using the Wigner phase-space distribution. While it does not furnish the 3D distributions with the probabilistic meaning, it allows us to treat their relativistic effects. Moreover, it shows that the 3D BF and 2D IMF distributions can naturally be interpolated in the Wigner sense. Thus, we can trace down the origin of the relativistic corrections to the 2D IMF distributions. At the same time, a direct connection between the 3D BF and 2D IMF distributions was found to be the IMF Abel transform [64,65]. Note that, very recently, a novel concept of the 3D strict probabilistic distribution was introduced to remove ambiguous relativistic corrections [66,67]. In this work, we first define the 3D BF distributions in the Wigner sense and then map out the 2D IMF ones by using the IMF Abel transform.

In the current work, we will scrutinize the GFFs of the baryon octet and pertinent three-dimensional distributions within the framework of a pion mean-field approach or the chiral quark-soliton model (χQSM) [68–70]. E. Witten in his seminal paper [71,72] inspired the idea of the meson mean-field approach. In the limit of a large number of colors (N_c), the quantum fluctuations are of order $1/N_c$, so that it can be ignored. Thus, a baryon can be viewed as N_c valence quarks bound by a pion mean field that arises from a classical solution of the equation of motion. To put more explicitly, the presence of the N_c valence quarks polarizes the vacuum, which produces the pion mean field. Then the N_c valence quarks are also influenced by the pion mean field in a self-consistent way. As a result, a classical baryon appears as a chiral soliton with a hedgehog symmetry, which is composed of the N_c valence quarks. While we ignore the $1/N_c$ mesonic quantum fluctuations, we have to consider the fluctuations of the pion field along the zero-mode direction. The translational and rotational zero modes are related to the symmetries of the baryon. Integrating over the zero modes completely, we can restore the correct quantum numbers of the baryon [68,70]. The χQSM successfully described various properties of the baryon octet and decuplet such as the EM properties [73–79], axial-vector structures [80–82], tensor charges [83,84], GFFs [65,85–88], and partonic structures [89–97]. It has also been extended to singly heavy baryons [98–106]. The GFFs of the singly heavy baryons were also studied within the χQSM [88]. The χQSM can also be associated with quantum chromodyanmics (QCD) via the instanton vacuum [107,108]. The low-energy QCD effective partition function can be derived from the instanton vacuum. The dynamical quark mass, which is obtained from the Fourier transform of the fermionic zero mode, is originally momentum dependent. In the present work, we turn off the momentum dependence and introduce a regularization scheme to tame the divergence coming from the quark loops.

The present work is organized as follows: In Sec. II, we define the GFFs of a spin-1/2 baryon from the matrix elements of the EMT current. In Sec. III A, we explain the general formalism for the EMT distributions in both 3D and 2D cases. In Sec. IV, we show how the GFFs and the EMT distributions can be computed within a framework of the SU(3) χQSM, considering the effects of the flavor SU(3) symmetry breaking. In Sec. V, the numerical results for the GFFs and the EMT distributions of the octet baryons are presented and discussed. The last section is devoted to the summary of the present work and draws conclusions.

II. GRAVITATIONAL FORM FACTORS OF A SPIN-1/2 PARTICLE

The symmetric EMT current in QCD can be derived by varying the QCD action under the Poincaré transformation according to Nöther's theorem with the symmetrization imposed for a particle with nonzero spin [109–111]. More directly, one can derive the symmetric EMT current by taking a functional derivative of the QCD action [1,112] with respect to the metric tensor of a curved background field. The symmetric total EMT operator consists of the quark (q) and gluon (g) parts, which are, respectively, expressed as

$$\hat{T}_q^{\mu\nu} = \frac{i}{4}\left[\bar{\psi}_q\gamma^\mu\vec{\mathcal{D}}^\nu\psi_q + \bar{\psi}_q\gamma^\nu\vec{\mathcal{D}}^\mu\psi_q - \bar{\psi}_q\gamma^\mu\overleftarrow{\mathcal{D}}^\nu\psi_q - \bar{\psi}_q\gamma^\nu\overleftarrow{\mathcal{D}}^\mu\psi_q\right] - g^{\mu\nu}\bar{\psi}_q\left(\frac{i}{2}\vec{\not{\mathcal{D}}} - \frac{i}{2}\overleftarrow{\not{\mathcal{D}}} - \hat{m}_q\right)\psi_q,$$
$$\hat{T}_g^{\mu\nu} = F^{a,\mu\eta}F^{a,\nu}_{\ \ \eta} + \frac{1}{4}g^{\mu\nu}F^{a,\kappa\eta}F^{a,}_{\ \ \kappa\eta}. \quad (1)$$

Here, the covariant derivatives are defined as $\vec{\mathcal{D}}_\mu = \vec{\partial}_\mu + igt^aA^a_\mu$ and $\overleftarrow{\mathcal{D}}_\mu = \overleftarrow{\partial}_\mu - igt^aA^a_\mu$. t^a represent the SU(3) color group generators that satisfy the commutation relations $[t^a, t^b] = if^{abc}t^c$ and are normalized to be $\mathrm{tr}(t^at^b) = \frac{1}{2}\delta^{ab}$. ψ_q denotes the quark field with flavor q and $\hat{m}_q$ designates the corresponding current quark mass. $F^{a,\mu\eta}$ stands for the gluon field strength expressed as $F^a_{\mu\nu} = \partial_\mu A^a_\nu - \partial_\nu A^a_\mu - gf^{abc}A^b_\mu A^c_\nu$. The total EMT operator is conserved as follows:

$$\partial^\mu\hat{T}_{\mu\nu} = 0, \qquad \hat{T}^{\mu\nu} = \sum_q \hat{T}_q^{\mu\nu} + \hat{T}_g^{\mu\nu}. \quad (2)$$

For the lowest-lying octet baryon, the matrix element of the EMT current can be parametrized in terms of the three GFFs [1,2,113]:

$$\langle B, p', J_3'|\hat{T}_{\mu\nu}(0)|B, p, J_3\rangle = \bar{u}(p', J_3')\left[A^B(t)\frac{P_\mu P_\nu}{m_B} + J^B(t)\frac{i(P_\mu\sigma_{\nu\rho} + P_\nu\sigma_{\mu\rho})\Delta^\rho}{2m_B} + D^B(t)\frac{\Delta_\mu\Delta_\nu - g_{\mu\nu}\Delta^2}{4m_B}\right]u(p, J_3), \quad (3)$$

which depends on the spin polarizations J_3 and J_3', the average momentum $P = (p + p')/2$ of the initial and final states, and the four-momentum transfer $\Delta = p' - p$. The squared momentum transfer is denoted by $t = \Delta^2$. The on-shell conditions of the final and initial four momenta are given by $p'^2 = p^2 = m_B^2$, where m_B denotes the mass of the octet baryon. In the BF, these GFFs $A^B(t)$, $J^B(t)$, and $D^B(t)$ are traditionally understood as the mass, angular momentum, and D-term form factors, respectively. Here, one should keep in mind that in the level of the quark and gluon degrees of freedom we have one additional form factor $\bar{c}$, which is constrained to satisfy the relation $\sum_{a=q,g}\bar{c}^a(t) = 0$. It can be dropped because of the conservation of the total EMT current.

III. ENERGY-MOMENTUM TENSOR DISTRIBUTIONS

In the BF, a 3D distribution is traditionally defined as a Fourier transformation of the corresponding form factor. Since, however, the baryon cannot be localized below the Compton wavelength, it causes ambiguous relativistic corrections. These corrections are up to 20% for the nucleon. In the nonrelativistic picture, they are often neglected. In the large N_c limit, the frame dependence of the distribution was carefully examined in Ref. [114]. These 3D distributions in the BF can be understood as quasiprobabilistic distributions in phase space or as the Wigner distributions [26,115–117]. To obtain the quantum-mechanical probabilistic distributions, one should take the IMF or the LF frame such that the relativistic corrections are kinematically suppressed and the nucleon is described as a transversely localized state. This yields 2D transverse densities in the IMF or on the LF.

The matrix element of the EMT current for a physical state $|\psi\rangle$ can be expressed in terms of the Wigner distribution as [116]

$$\langle\hat{T}^{\mu\nu}(\boldsymbol{r})\rangle = \int\frac{d^3\boldsymbol{P}}{(2\pi)^3}\int d^3\boldsymbol{R}W(\boldsymbol{R},\boldsymbol{P})\langle\hat{T}^{\mu\nu}(\boldsymbol{r})\rangle_{\boldsymbol{R},\boldsymbol{P}}, \quad (4)$$

where $W(\boldsymbol{R},\boldsymbol{P})$ represents the Wigner distribution given by

$$W(\boldsymbol{R},\boldsymbol{P}) = \int\frac{d^3\boldsymbol{\Delta}}{(2\pi)^3}e^{-i\boldsymbol{\Delta}\cdot\boldsymbol{R}}\tilde{\psi}^*\left(\boldsymbol{P} + \frac{\boldsymbol{\Delta}}{2}\right)\tilde{\psi}\left(\boldsymbol{P} - \frac{\boldsymbol{\Delta}}{2}\right), = \int d^3\boldsymbol{z}e^{-i\boldsymbol{z}\cdot\boldsymbol{P}}\psi^*\left(\boldsymbol{R} - \frac{\boldsymbol{z}}{2}\right)\psi\left(\boldsymbol{R} + \frac{\boldsymbol{z}}{2}\right). \quad (5)$$

The average position $\boldsymbol{R}$ and momentum $\boldsymbol{P}$ are defined as $\boldsymbol{R} = (\boldsymbol{r}' + \boldsymbol{r})/2$ and $\boldsymbol{P} = (\boldsymbol{p}' + \boldsymbol{p})/2$, respectively. $\boldsymbol{\Delta} = \boldsymbol{p}' - \boldsymbol{p}$ denotes the three-momentum transfer, which enables us to get access to the internal structure of a particle. The variable $\boldsymbol{z} = \boldsymbol{r}' - \boldsymbol{r}$ stands for the position separation between the initial and final particles. The Wigner distribution contains information on the wave packet of a particle

$$\psi(\boldsymbol{r}) = \langle\boldsymbol{r}|\psi\rangle = \int\frac{d^3\boldsymbol{p}}{(2\pi^3)}e^{i\boldsymbol{p}\cdot\boldsymbol{r}}\tilde{\psi}(\boldsymbol{p}),$$
$$\tilde{\psi}(\boldsymbol{p}) = \frac{1}{\sqrt{2p^0}}\langle p|\psi\rangle, \quad (6)$$

where the plane wave states $|p\rangle$ and $|\boldsymbol{r}\rangle$ are, respectively, normalized as $\langle p'|p\rangle = 2p^0(2\pi)^3\delta^{(3)}(\boldsymbol{p}' - \boldsymbol{p})$ and $\langle\boldsymbol{r}'|\boldsymbol{r}\rangle = \delta^{(3)}(\boldsymbol{r}' - \boldsymbol{r})$. The position state $|\boldsymbol{r}\rangle$ localized at $\boldsymbol{r}$ at time $t = 0$ is defined as a Fourier transform of the momentum eigenstate $|p\rangle$

$$|\boldsymbol{r}\rangle = \int\frac{d^3\boldsymbol{p}}{(2\pi)^3\sqrt{2p^0}}e^{-i\boldsymbol{p}\cdot\boldsymbol{r}}|p\rangle. \quad (7)$$

If we integrate over the average position and momentum, then the probabilistic density in either position or momentum space is recovered to be

$$\int \frac{d^3\boldsymbol{P}}{(2\pi)^3} W_N(\boldsymbol{R},\boldsymbol{P}) = |\psi_N(\boldsymbol{R})|^2, \qquad \int d^3\boldsymbol{R} W_N(\boldsymbol{R},\boldsymbol{P}) = |\tilde{\psi}_N(\boldsymbol{P})|^2. \tag{8}$$

Given $\boldsymbol{P}$ and $\boldsymbol{R}$, the matrix element $\langle \hat{T}^{\mu\nu}(\boldsymbol{r})\rangle_{\boldsymbol{R},\boldsymbol{P}}$ conveys information on the internal structure of the particle localized around the average position $\boldsymbol{R}$ and average momentum $\boldsymbol{P}$. This can be expressed as the 3D Fourier transform of the matrix element $\langle B, p', J'_3|\hat{T}^{\mu\nu}(0)|B, p, J_3\rangle$:

$$\langle \hat{T}^{\mu\nu}(\boldsymbol{r})\rangle_{\boldsymbol{R},\boldsymbol{P}} = \langle \hat{T}^{\mu\nu}(0)\rangle_{-\boldsymbol{x},\boldsymbol{P}} = \int \frac{d^3\boldsymbol{\Delta}}{(2\pi)^3} e^{-i\boldsymbol{x}\cdot\boldsymbol{\Delta}} \frac{1}{\sqrt{2p^0}\sqrt{2p'^0}} \langle p', J'_3|\hat{T}^{\mu\nu}(0)|p, J_3\rangle, \tag{9}$$

with the shifted position vector $\boldsymbol{x} = \boldsymbol{r} - \boldsymbol{R}$. Note that, very recently, a novel concept of the 3D strict probabilistic distribution was introduced to remove ambiguous relativistic corrections [66,67].

A. Three-dimensional energy-momentum tensor distributions in the Breit frame

Having integrated over $\boldsymbol{P}$ of Eq. (4), we find that the part of the wave packet can be factorized. Thus, the target in the BF is understood as a localized state around $\boldsymbol{R}$ from the Wigner perspective. In this frame, Eq. (9) is reduced to

$$T^{\mu\nu}_{\mathrm{BF},B}(\boldsymbol{r}, J'_3, J_3) = \int \frac{d^3\Delta}{(2\pi)^3 2P_0} e^{-i\boldsymbol{\Delta}\cdot\boldsymbol{r}} \langle B, p', J'_3|\hat{T}^{\mu\nu}(0)|B, p, J_3\rangle. \tag{10}$$

From now on we use $\boldsymbol{r}$ instead of $\boldsymbol{x}$, i.e., $\boldsymbol{x} = \boldsymbol{r} - \boldsymbol{R} \to \boldsymbol{r}$. In the Wigner sense, the temporal component of the EMT current yields mass distribution:

$$T^{00}_{\mathrm{BF},B}(\boldsymbol{r}, J'_3, J_3) = \varepsilon^B(r)\delta_{J'_3 J_3} = m_B \int \frac{d^3\Delta}{(2\pi)^3} e^{-i\boldsymbol{\Delta}\cdot\boldsymbol{r}} \left[A^B(t) - \frac{t}{4m_B^2}(A^B(t) - 2J^B(t) + D^B(t))\right]\delta_{J'_3 J_3}. \tag{11}$$

By integrating $T^{00}_{\mathrm{BF},B}$ over 3D space, one obviously gets the mass of a baryon in the rest frame

$$\int d^3r T^{00}_{\mathrm{BF},B}(\boldsymbol{r}, J'_3, J_3) = m_B A^B(0) = m_B, \tag{12}$$

with the normalization $A^B(0) = 1$. Note that, for a higher-spin particle ($J \geq 1$), a quadrupole distribution of the energy inside the particle appears [46–49,56,118,119]. The size of the mass distribution can be quantified by the mass radius. It is given by either integral of the mass distribution or derivative of the mass form factor $A^B(t)$ with respect to the momentum squared,

$$\langle r^2_\varepsilon\rangle_B = \frac{\int d^3r r^2 \varepsilon^B(r)}{\int d^3r \varepsilon^B(r)} = \frac{6}{A^B(0)} \frac{dA^B(t)}{dt}\bigg|_{t=0}. \tag{13}$$

The $0k$ component of the EMT current is related to the spatial distribution of the spin carried by the partons inside a baryon:

$$\begin{aligned} J^i_B(\boldsymbol{r}, J'_3, J_3) &= \epsilon^{ijk} r^j T^{0k}_{\mathrm{BF},B}(\boldsymbol{r}, J'_3, J_3), \\ &= 2S^j_{J'_3 J_3} \int \frac{d^3\Delta}{(2\pi)^3} e^{-i\boldsymbol{\Delta}\cdot\boldsymbol{r}} \left[\left(J^B(t) + \frac{2}{3} t \frac{J^B(t)}{dt}\right)\delta^{ij} + \left(\Delta^i\Delta^j - \frac{1}{3}\boldsymbol{\Delta}^2\delta^{ij}\right)\frac{J^B(t)}{dt}\right]. \end{aligned} \tag{14}$$

In principle, both the monopole and quadrupole distributions should be considered when we deal with the spin distribution. However, we drop the quadrupole contribution for simplicity, which does not affect the normalization of the spin form factor $J^B(0)$. The quadrupole structure of the spin distribution was intensively discussed and related to the monopole distribution in Refs. [120,121]. The monopole contribution to the spin distribution, which is the first term in Eq. (14), is defined as

$$\rho_J^B(r) \coloneqq \int \frac{d^3\Delta}{(2\pi)^3} e^{-i\boldsymbol{\Delta}\cdot\boldsymbol{r}} \left[\left(J^B(t) + \frac{2}{3} t \frac{J^B(t)}{dt} \right) \right]. \quad (15)$$

Integrating $J_B^i(\boldsymbol{r}, J_3', J_3)$ over space gives the spin of the baryon as follows

$$\begin{aligned} \int d^3r J_B^i(\boldsymbol{r}, J_3', J_3) &= 2\hat{S}^i_{J_3' J_3} \int d^3r \rho_J^B(r) \\ &= 2\hat{S}^i_{J_3' J_3} J^B(0) = \hat{S}^i_{J_3' J_3}, \end{aligned} \quad (16)$$

which is just the spin operator of a baryon. The quadrupole contribution, the second term in Eq. (14), obviously vanishes after the integration over the 3D space.

The spatial components EMT current $T^{ij}_{\mathrm{BF},B}$ provides information on the mechanical properties of a baryon. It can be decomposed into isotropic and anisotropic contributions. This anisotropic contribution plays a significant role in the mechanical structure of a baryon [26,113]. They are, respectively, referred to as the pressure $p^B(r)$ and shear force $s^B(r)$ and expressed as [58,113]

$$T^{ij}_{\mathrm{BF},B}(\boldsymbol{r}, J_3', J_3) = p^B(r)\delta^{ij}\delta_{J_3' J_3} + s^B(r)\left(\frac{r^i r^j}{r^2} - \frac{1}{3}\delta^{ij} \right) \delta_{J_3' J_3}, \quad (17)$$

where the pressure and shear force distributions are, respectively, defined as

$$\begin{aligned} p^B(r) &= \frac{1}{6m_B} \frac{1}{r^2} \frac{1}{dr} r^2 \frac{d}{dr} \tilde{D}^B(r), \\ s^B(r) &= -\frac{1}{4m_B} r \frac{d}{dr} \frac{1}{r} \frac{d}{dr} \tilde{D}^B(r), \quad \text{with} \\ \tilde{D}^B(r) &= \int \frac{d^3\Delta}{(2\pi)^3} e^{-i\boldsymbol{\Delta}\cdot\boldsymbol{r}} D^B(t). \end{aligned} \quad (18)$$

From Eq. (18), it is easy to see that the 3D von Laue stability condition for the pressure is automatically satisfied:

$$\int d^3r p^B(r) = 0. \quad (19)$$

It indicates that the pressure should have at least one nodal point. In addition, the pressure and shear force distributions automatically comply with the differential equation derived from the total EMT conservation:

$$\begin{aligned} \partial^i T^{ij}_{\mathrm{BF},B}(\boldsymbol{r}, J_3', J_3) = \frac{r^j}{r} \Bigg[&\frac{2}{3} \frac{\partial s^B(r)}{\partial r} + \frac{2 s^B(r)}{r} \\ &+ \frac{\partial p^B(r)}{\partial r} \Bigg] \delta_{J_3' J_3} = 0. \end{aligned} \quad (20)$$

It gives a number of the integral relations between pressure and shear force. One of them is the 2D von Laue stability condition that is derived as

$$\int_0^\infty dr\, r \left(-\frac{1}{3} s^B(r) + p^B(r) \right) = 0. \quad (21)$$

The combination $-\frac{1}{3}s^B(r) + p^B(r)$ carries the meaning of the tangential force distribution. It is an eigenvalue of the stress tensor and it must at least have one nodal point such that it complies with the 2D von Laue condition (21).

Moreover, in Refs. [26,113,122], the local stability conditions were conjectured:

$$\frac{2}{3} s^B(r) + p^B(r) > 0, \qquad s^B(r) > 0. \quad (22)$$

The combination $\frac{2}{3}s^B(r) + p^B(r)$ bears the meaning of the normal force distribution and is again identified as an eigenvalue of the stress tensor. Equation (22) implies that at any distance r the normal force should be directed outwards. This Polyakov-Schweitzer local stability condition was examined in various contexts [26,88,113,122]. The value of the D-term form factor at zero momentum transfer is obtained by integrating the pressure or shear-force distributions over 3D space as

$$D^B(0) = -\frac{4m_B}{15} \int d^3r r^2 s^B(r) = m_B \int d^3r r^2 p^B(r), \quad (23)$$

and the positive shear force for any value of r implies the negative D term. In addition, the positivity of the normal forces (22) enables us to define the mechanical radius:

$$\langle r^2_{\mathrm{mech}} \rangle_B = \frac{\int d^3r r^2 (\frac{2}{3} s^B(r) + p^B(r))}{\int d^3r (\frac{2}{3} s^B(r) + p^B(r))} = \frac{6D^B(0)}{\int_{-\infty}^0 D^B(t) dt}. \quad (24)$$

B. Two-dimensional energy-momentum tensor distributions in the infinite momentum frame

In Refs. [26,116], the elastic frame (EF) was introduced. This frame naturally interpolates between the 2D BF and 2D IMF for both the nucleon [116,123] and the deuteron [117]. In the EF, the average momentum and momentum transfer of the initial and final states are, respectively, given by $P = (P_0, \mathbf{0}_\perp, P_z)$ and $\Delta = (0, \boldsymbol{\Delta}_\perp, 0)$. Accordingly, the EF distributions depend on the impact parameter $x_\perp$ ($\boldsymbol{r} = (\boldsymbol{x}_\perp, x_z)$) and momentum $\boldsymbol{P} = (\mathbf{0}, P_z)$, where an octet baryon moves along the z direction without loss of generality. In this frame, Eq. (9) is reduced to

$$T^{\mu\nu}_{\mathrm{EF},B}(\boldsymbol{x}_\perp, P_z, J'_3, J_3) = \int \frac{d^2\boldsymbol{\Delta}_\perp}{2P_0(2\pi)^2} e^{-i\boldsymbol{x}_\perp\cdot\boldsymbol{\Delta}_\perp} \langle B, p', J'_3|\hat{T}^{\mu\nu}(0)|B, p, J_3\rangle\Big|_{\Delta_z=0}. \tag{25}$$

To proceed to the IMF from the EF, we set $P_z \to \infty$ in Eq. (25). As explored in Refs. [26,26,42,42,64,120,121], we obtain the 2D IMF or 2D LF EMT distributions by taking the limit $P_z \to \infty$. Note that we only consider the longitudinally polarized octet baryons instead of the transversely polarized ones. As a result, the corresponding 2D distributions for the mass $\mathcal{E}^B(x_\perp)$, angular momentum $\rho_J^{(2D),B}(x_\perp)$, pressure $\mathcal{P}^B(x_\perp)$, and shear force $\mathcal{S}^B(x_\perp)$ are obtained by the 2D inverse Fourier transform

$$\begin{aligned}
&\mathcal{E}^B(x_\perp) = m_B\tilde{A}^B(x_\perp), \qquad \rho_J^{(2D),B}(x_\perp) = -\frac{1}{2}x_\perp\frac{d}{dx_\perp}\tilde{J}^B(x_\perp),\\
&\mathcal{S}^B(x_\perp) = -\frac{1}{8m_B}x_\perp\frac{1}{dx_\perp}\frac{1}{x_\perp}\frac{d}{dx_\perp}\tilde{D}^B(x_\perp), \qquad \mathcal{P}^B(x_\perp) = \frac{1}{16m_B}\frac{1}{x_\perp}\frac{d}{dx_\perp}x_\perp\frac{d}{dx_\perp}\tilde{D}^B(x_\perp),
\end{aligned} \tag{26}$$

where the 2D Fourier transform of the corresponding GFFs are defined as follows

$$\tilde{F}^B(x_\perp) = \int \frac{d^2\boldsymbol{\Delta}_\perp}{(2\pi)^2} e^{-i\boldsymbol{\Delta}_\perp\cdot\boldsymbol{x}_\perp} F^B(-\boldsymbol{\Delta}_\perp^2), \tag{27}$$

with $F^B = A^B, J^B, D^B$. In the IMF, we divide the mass and mechanical densities, respectively, by the Lorentz factors P_0/m_B and $2m_B/P_0$ to remove the kinematical divergence and suppression in these densities [64,65]. On the other hand, since the longitudinal boost does not mix the longitudinal component of the angular momentum, its distribution does not need to have an additional Lorentz factor [120]. In addition, since the $\mathcal{E}^B$ is normalized to the mass of an octet baryon, we refer to it as "mass distribution" instead of the "momentum distribution." It is different from the higher-twist mass distribution that arises from the "bad" component of the EMT current.

These distributions (26) defined in the IMF can be related to those in the 3D BF (11), (15), and (18) through the IMF Abel transform [64,65] as follows:

$$\begin{aligned}
\left(1 - \frac{\partial^2_{(2D)}}{4m_B^2}\right)\mathcal{E}^B(x_\perp) &= 2\int_{x_\perp}^\infty \frac{rdr}{\sqrt{r^2-x_\perp^2}}\left[\varepsilon^B(r) + \frac{3}{2}p^B(r) + \frac{3}{2m_B}\frac{1}{r^2}\frac{d}{dr}r\rho_J^B(r)\right],\\
\rho_J^{(2D),B}(x_\perp) &= 3\int_{x_\perp}^\infty \frac{\rho_J^B(r)}{r}\frac{x_\perp^2 dr}{\sqrt{r^2-x_\perp^2}},\\
\mathcal{S}^B(x_\perp) &= \int_{x_\perp}^\infty \frac{s^B(r)}{r}\frac{x_\perp^2 dr}{\sqrt{r^2-x_\perp^2}},\\
\frac{1}{2}\mathcal{S}^B(x_\perp) + \mathcal{P}^B(x_\perp) &= \frac{1}{2}\int_{x_\perp}^\infty \left(\frac{2}{3}s^B(r) + p^B(r)\right)\frac{rdr}{\sqrt{r^2-x_\perp^2}}.
\end{aligned} \tag{28}$$

They convey the same physical meaning from the 3D distributions to the 2D ones. Integrating those distributions over the transversal plane $\boldsymbol{x}_\perp$, we obtain

$$\int d^2x_\perp \mathcal{E}^B(x_\perp) = m_B A^B(0), \qquad \int d^2x_\perp \rho_J^{(2D)}(x_\perp) = J^B(0), \tag{29}$$

with the normalized form factor $A^B(0) = 1$ and $J^B(0) = 1/2$, respectively. We can define the 2D mass radius in the same manner as the 3D one, which are related each other as follows

$$\langle x^2_{\perp\mathcal{E}}\rangle_B = \frac{1}{m_B}\int d^2x_\perp x_\perp^2 \mathcal{E}^B(x_\perp) = \frac{2}{3}\langle r_\varepsilon^2\rangle_B + \frac{D^B(0)}{m_B^2}. \tag{30}$$

Interestingly, because of the Lorentz boost effects, the 2D mass radius is associated with to the mechanical properties, i.e., the D term.

The conservation of the EMT current also furnishes the 2D stability condition of the nucleon. We can easily derive the 2D equilibrium equation from the conservation of the EMT current

$$\mathcal{P}^{B\prime}(x_\perp)+\frac{\mathcal{S}^B(x_\perp)}{x_\perp}+\frac{1}{2}\mathcal{S}^{B\prime}(x_\perp)=0, \tag{31}$$

which is similar to the 3D case. One can clearly see that Eq. (26) satisfies the equilibrium equation (31). In addition, the 2D pressure distribution complies with the 2D von Laue condition and that of its lower dimension subsystem in the octet baryon as

$$\int d^2x_\perp \mathcal{P}^B(x_\perp)=0, \quad \int_0^\infty dx_\perp\left[\mathcal{P}^B(x_\perp)-\frac{1}{2}\mathcal{S}^B(x_\perp)\right]=0. \tag{32}$$

Furthermore, the Polyakov-Schweitzer local stability condition for the 3D [122] and 2D [42] pressure and shear force distributions can be considered. The 3D normal force directed outward implies that the 2D normal force should also be directed outward

$$\frac{1}{2}\mathcal{S}(x_\perp)+\mathcal{P}(x_\perp)>0 \tag{33}$$

as shown in Eq. (28).

Note that the combination $\frac{1}{2}\mathcal{S}^B(x_\perp)+\mathcal{P}^B(x_\perp)$ and $-\frac{1}{2}\mathcal{S}^B(x_\perp)+\mathcal{P}^B(x_\perp)$ mean the normal and tangential force distributions in the 2D IMF, respectively. The positivity of the 2D normal force is guaranteed by the fact that the Abel image of a positive function is also positive and vice versa. This implies that the positivity of the 3D local stability condition is equivalent to the 2D ones. Thus, it enables us directly to relate the 3D mechanical radius to the 2D one

$$\begin{aligned}\langle x^2_{\perp\mathrm{mech}}\rangle_B &= \frac{\int d^2x_\perp x_\perp^2(\frac{1}{2}\mathcal{S}^B(x_\perp)+\mathcal{P}^B(x_\perp))}{\int d^2x_\perp(\frac{1}{2}\mathcal{S}^B(x_\perp)+\mathcal{P}^B(x_\perp))}\\ &= \frac{4D^B(0)}{\int_{-\infty}^0 dtD^B(t)}=\frac{2}{3}\langle r^2_{\mathrm{mech}}\rangle_B.\end{aligned} \tag{34}$$

IV. GRAVITATIONAL FORM FACTORS OF THE BARYON OCTET IN THE SU(3) CHIRAL QUARK-SOLITON MODEL

We start from the low-energy effective partition function in Euclidean space

$$\begin{aligned}\mathcal{Z}_{\chi\mathrm{QSM}} &= \int \mathcal{D}\psi\mathcal{D}\psi^\dagger\mathcal{D}U\exp\left[\int d^4x\psi^\dagger D(U)\psi\right],\\ &= \int \mathcal{D}U\exp\left[-S_{\mathrm{eff}}(U)\right],\end{aligned} \tag{35}$$

where S_{eff} is the effective chiral action

$$S_{\mathrm{eff}}(U)=-N_c\mathrm{Tr}\ln D(U). \tag{36}$$

The Dirac operator $D(U)$ is defined by

$$D(U)=i\partial\!\!\!/+i\hat{m}+iMU^{\gamma_5}, \tag{37}$$

where $\hat{m}$ represents the diagonal matrix of the current quark masses, i.e., $\hat{m}=\mathrm{diag}(m_u,m_d,m_s)$, in the SU(3) flavor space. Assuming isospin symmetry, we set the current quark masses of u and d quarks to be equal, i.e., $m_u=m_d$. So, the matrix of the current quark masses is written as

$$\hat{m}=m_0\mathbf{1}+m_8\lambda^8, \tag{38}$$

where m_0 and m_8, respectively, stand for the singlet and octet components of the current quark mass matrix. They are written as

$$m_0=\frac{2\bar{m}+m_s}{3}, \qquad m_8=\frac{\bar{m}-m_s}{\sqrt{3}}. \tag{39}$$

By introducing the average current quark mass $\bar{m}=(m_u+m_d)/2$, we can rewrite the matrix of the current quark masses in terms of δm that will be treated perturbatively:

$$\delta m=\hat{m}-\bar{m}=(m_0\mathbf{1}-\bar{m})+m_8\lambda^8=M_1\mathbf{1}+M_8\lambda^8, \tag{40}$$

with $M_1=m_0-\bar{m}$ and $M_8=m_8$. M stands for the dynamical quark mass in Eq. (37). Note that the original dynamical quark mass depends on the quark momentum k. It is derived from the zero-mode quark solution in the QCD instanton vacuum [107,108] and plays a role of the natural regulator for a quark loop. Since we turn off the momentum dependence for simplicity, it is necessary to introduce an explicit regularization scheme. Here, we use the proper-time regularization.

U^{γ_5} denotes the SU(3) chiral field, which is defined by

$$U^{\gamma_5}=\frac{1+\gamma_5}{2}U+\frac{1-\gamma_5}{2}U^\dagger \tag{41}$$

with

$$U=\exp[i\pi^a\lambda^a], \tag{42}$$

where π^a represents the pseudo-Nambu-Goldstone fields and λ^a are the Gell-Mann matrices.

Introducing the hedgehog symmetry in flavor SU(2), we regard each pion field with $a=1,2,3$ as being aligned along the corresponding 3D space

$$\pi^a(\boldsymbol{r})=\hat{n}^aP(r), \tag{43}$$

where $\hat{n}^a = x^a/r$ with $r = |\boldsymbol{r}|$. $P(r)$ is the profile function of the chiral soliton. It will be determined by solving the classical equation of motion self-consistently. The SU(2) chiral field is expressed as

$$U^{\gamma_5}_{\mathrm{SU}(2)} = \exp[i\gamma_5 \hat{\boldsymbol{n}} \cdot \boldsymbol{\tau} P(r)]. \tag{44}$$

To construct the chiral soliton in flavor SU(3), we embed the SU(2) soliton into the SU(3) one [72]:

$$U^{\gamma_5} = \begin{pmatrix} U^{\gamma_5}_{\mathrm{SU}(2)} & 0 \\ 0 & 1 \end{pmatrix}. \tag{45}$$

The Dirac Hamiltonian $h(U)$ is defined by

$$h(U) = \gamma_4 \gamma_i \partial_i + \gamma_4 M U^{\gamma_5} + \gamma_4 \bar{m} \mathbf{1}. \tag{46}$$

The corresponding eigenenergies and eigenfunctions are obtained by diagonalizing the one-body Dirac Hamiltonian

$$h(U)\psi_n(\boldsymbol{r}) = E_n \psi_n(\boldsymbol{r}), \tag{47}$$

where E_n and $\psi_n(\boldsymbol{r})$ denote the eigenenergies and eigenfunctions of the Hamiltonian $h(U)$, respectively.

Since we employ the saddle-point approximation in the large N_c limit, we can easily perform the integration over U in Eq. (35). The result is simply given by the value of the integrand at the stationary mesonic configuration, which can be found by solving the saddle point equation $\delta S_{\mathrm{eff}}/\delta P(r) = 0$. By minimizing self-consistently the energy around the saddle point of the pion mean field, we obtain the classical soliton mass (see review [70] in detail), which is expressed as

$$M_{\mathrm{sol}} = N_c E_{\mathrm{val}} + E_{\mathrm{sea}}. \tag{48}$$

Here, E_{val} is the energy of the discrete bound level, and E_{sea} is the sum of the Dirac-continuum energies.

In the χQSM, the symmetrized EMT current is derived as

$$\hat{T}^{\mu\nu}_{\mathrm{eff}}(x) = -\frac{i}{4}\psi^\dagger(x)(i\gamma^\mu \overrightarrow{\partial}^\nu + i\gamma^\nu \overrightarrow{\partial}^\mu - i\gamma^\mu \overleftarrow{\partial}^\nu - i\gamma^\nu \overleftarrow{\partial}^\mu)\psi(x), \tag{49}$$

and the matrix element of this EMT current can be computed as follows:

$$\langle B, p', J'_3|\hat{T}^{\mu\nu}_{\mathrm{eff}}(0)|B, p, J_3\rangle = N^*(\boldsymbol{p}')N(\boldsymbol{p}) \lim_{T\to\infty} \exp\left(-i(p'+p)\frac{T}{2}\right) \int d^3\boldsymbol{x} d^3\boldsymbol{y} \exp(-i\boldsymbol{p}'\cdot\boldsymbol{y} + i\boldsymbol{p}\cdot\boldsymbol{x})$$
$$\times \int \mathcal{D}\psi\mathcal{D}\psi^\dagger\mathcal{D}U J_B(\boldsymbol{y}, T/2) T^{\mu\nu}_{\mathrm{eff}}(0) J^\dagger_B(\boldsymbol{x}, -T/2) \exp\left[\int d^4z \psi^\dagger(z) D(U) \psi(z)\right], \tag{50}$$

where the baryon states $|B(p, J_3)\rangle$ and $\langle B(p', J'_3)|$ are, respectively, defined as

$$|B, p, J_3\rangle = \lim_{x_4\to-\infty} \exp(ip_4 x_4) N(\boldsymbol{p}) \int d^3\boldsymbol{x} \exp(i\boldsymbol{p}\cdot\boldsymbol{x}) J^\dagger_B(\boldsymbol{x}, x_4)|0\rangle,$$
$$\langle B, p', J'_3| = \lim_{y_4\to\infty} \exp(-ip'_4 y_4) N^*(\boldsymbol{p}') \int d^3\boldsymbol{y} \exp(-i\boldsymbol{p}'\cdot\boldsymbol{y})\langle 0|J_B(\boldsymbol{y}, y_4). \tag{51}$$

J_B represents the Ioffe-type current consisting of the N_c valence quarks [124]

$$J_B(y) = \frac{1}{N_c!}\epsilon_{\alpha_1\cdots\alpha_{N_c}} \Gamma^{f_1\cdots f_{N_c}}_{(TT_3Y)(JJ'_3Y_R)} \psi_{f_1\alpha_1}(y)\cdots\psi_{f_{N_c}\alpha_{N_c}}(y),$$
$$J^\dagger_B(x) = \frac{1}{N_c!}\epsilon_{\beta 1\ldots\beta_{N_c}} \Gamma^{g_1\cdots g_{N_c}*}_{(TT_3Y)(JJ_3Y_R)} (-i\psi^\dagger(x)\gamma_4)_{g_1\beta 1}\cdots(-i\psi^\dagger(x)\gamma_4)_{g_{N_c}\beta_{N_c}}, \tag{52}$$

where the greek and latin indices, respectively, denote the color and spin-isospin ones. The matrices $\Gamma_{(TT_3Y)(JJ_3Y_R)}$ carry the spin and flavor quantum numbers of the corresponding baryon. The right hypercharge $Y_R = N_c/3$ with $N_c = 3$ selects the lowest-lying representations of the SU(3) baryons such as the baryon octet ($\mathbf{8}$) and decuplet ($\mathbf{10}$).

Having performed the zero-mode quantization, we obtain the collective Hamiltonian

$$H_{\mathrm{coll}} = H_{\mathrm{sym}} + H_{\mathrm{sb}}, \tag{53}$$

where

$$H_{\rm sym} = M_{\rm sol} + \frac{1}{2I_1}\sum_{i=1}^{3}\hat{J}_i^2 + \frac{1}{2I_2}\sum_{p=4}^{7}\hat{J}_p^2,$$
$$H_{\rm sb} = \alpha D_{88}^{(8)} + \beta\hat{Y} + \frac{\gamma}{\sqrt{3}}\sum_{i=1}^{3} D_{8i}^{(8)}\hat{J}_i. \tag{54}$$

I_1 and I_2 stand for the moments of inertia. $D_{ab}^{(8)}$ denotes the SU(3) Wigner D function. Three dynamical parameters α, β, and γ are related to the flavor SU(3) symmetry breaking and given as follows:

$$\alpha = \left(\frac{1}{\sqrt{3}}\frac{\Sigma_{\pi N}}{\bar{m}} - \sqrt{3}\frac{K_2}{I_2}Y_R\right)M_8, \qquad \beta = \sqrt{3}\frac{K_2}{I_2}M_8,$$
$$\gamma = -2\sqrt{3}\left(\frac{K_1}{I_1} - \frac{K_2}{I_2}\right)M_8, \tag{55}$$

where K_1 and K_2 are anomalous moments of inertia and $\Sigma_{\pi N}$ is the pion-nucleon Σ term. The collective wave function of a baryon with flavor (YTT_3) and spin $(Y_R J J_3)$ in the SU(3) representation μ is derived as

$$\psi^{(\mu)}_{(YTT_3)(Y_R J J_3)}(A) = \sqrt{\dim(\mu)}(-1)^{J_3 - Y_R/2} D^{(\mu)*}_{(YTT_3)(Y_R J - J_3)}(A), \tag{56}$$

where $\dim(\mu)$ denotes the dimension of the representation μ. In the presence of the flavor SU(3) symmetry breaking term $H_{\rm sb}$, the collective wave functions of the baryon octet should be mixed with those in higher representations. Thus, those for the baryon octet are derived as

$$|B_{\mathbf{8}_{1/2}}\rangle = |\mathbf{8}_{1/2}, B\rangle + c_{\overline{\mathbf{10}}}^{B}|\overline{\mathbf{10}}_{1/2}, B\rangle + c_{\mathbf{27}}^{B}|\mathbf{27}_{1/2}, B\rangle, \tag{57}$$

with the mixing parameters

$$c_{\overline{\mathbf{10}}}^{B} = c_{\overline{\mathbf{10}}}\begin{bmatrix}\sqrt{5}\\0\\\sqrt{5}\\0\end{bmatrix}, \qquad c_{\mathbf{27}}^{B} = c_{\mathbf{27}}\begin{bmatrix}\sqrt{6}\\3\\2\\\sqrt{6}\end{bmatrix}, \tag{58}$$

in the basis $[N, \Lambda, \Sigma, \Xi]$. The coefficients $c_{\overline{\mathbf{10}}}$ and $c_{\mathbf{27}}$ are expressed in terms of α and γ

$$c_{\overline{\mathbf{10}}} = -\frac{I_2}{15}\left(\alpha + \frac{1}{2}\gamma\right), \qquad c_{\mathbf{27}} = -\frac{I_2}{25}\left(\alpha - \frac{1}{6}\gamma\right). \tag{59}$$

The matrix elements of the various components of the EMT current are written as in the large N_c limit,

$$\langle B, p', J_3'|\hat{T}^{00}_{\rm eff}|B, p, J_3\rangle = 2m_B^2\left(A^B(t) - \frac{t}{4m_B^2}D^B(t)\right)\delta_{J_3' J_3},$$
$$\langle B, p', J_3'|\hat{T}^{ik}_{\rm eff}|B, p, J_3\rangle = \frac{1}{2}(\Delta^i\Delta^k - \delta^{ik}\boldsymbol{\Delta}^2)D^B(t)\delta_{J_3' J_3},$$
$$\langle B, p', J_3'|\hat{T}^{0k}_{\rm eff}|B, p, J_3\rangle = -2im_B\epsilon^{klm}\Delta^l\hat{S}^m_{J_3' J_3}J^B(t). \tag{60}$$

Having considered the rotational $1/N_c$ and linear m_s corrections, we obtain the final expressions of the GFFs for a octet baryon B as follows:

$$A^B(t) - \frac{t}{4m_B^2}D^B(t) = \frac{1}{m_B}\int d^3r\, j_0(r\sqrt{-t})\varepsilon^B(r),$$
$$D^B(t) = 4m_B\int d^3r\frac{j_2(r\sqrt{-t})}{t}s^B(r),$$
$$J^B(t) = 3\int d^3r\frac{j_1(r\sqrt{-t})}{r\sqrt{-t}}\rho_J^B(r), \tag{61}$$

where the corresponding 3D densities ε^B, s^B, and ρ_J^B are given by

$$\varepsilon^B(r) = \mathcal{E}(r) + \left(M_1 + \frac{1}{\sqrt{3}}M_8\langle D_{88}\rangle_B\right)(\mathcal{S}(r) - 2\mathcal{C}(r)),$$
$$s^B(r) = \mathcal{N}_1(\boldsymbol{r}) - 2\left(M_1 + \frac{1}{\sqrt{3}}M_8\langle D_{88}\rangle_B\right)\mathcal{N}_2(\boldsymbol{r}),$$
$$\rho_J^B(r) = -\frac{1}{2I_1}\mathcal{I}_1(\boldsymbol{r}) + 2M_8\langle D_{83}\rangle_B\left(\frac{K_1}{I_1}\mathcal{I}_1(\boldsymbol{r}) - \mathcal{K}_1(\boldsymbol{r})\right). \tag{62}$$

Here, $\langle\ldots\rangle_B$ denotes the matrix element of the collective operator for a baryon state B. The explicit expressions for the densities $\mathcal{E}$, $\mathcal{S}$, $\mathcal{C}$, $\mathcal{N}_1$, $\mathcal{N}_2$, $\mathcal{I}_1$, and $\mathcal{K}_1$ are listed in Appendix A.

V. RESULTS AND DISCUSSION

Before we discuss the numerical results for the EMT distributions and the GFFs of the baryon octet, we first describe how the parameters in the χQSM are fixed. Since the quark loops cause the divergences, we need to regularize them by introducing a cutoff mass Λ. It is fixed by reproducing the experimental data on the pion decay constant $f_\pi = 93$ MeV. All other quark loops such as the pion mass are tamed by this fixed value of Λ. The current u- and d-quark masses are determined to be $m_u = m_d = 17.6$ MeV by reproducing the pion mass $m_\pi = 140$ MeV (see Refs. [70,125] for details). In principle the only free parameter of the χQSM is the dynamical quark mass M. It is fixed by computing the various nucleon form factors and mass splitting between light baryons [70]. The most preferable value is found to be 420 MeV. Since we are interested in the effect of flavor SU(3) symmetry breaking on the GFFs and EMT distributions, we need to fix the

value of the strange current quark mass. We employ it as $m_s = 180$ MeV, which describes the mass splitting of both the light and singly heavy baryons [70,100] very well. Note that we consider the linear m_s corrections.

The rotational and translational zero modes yield the $1/N_c$ corrections. While the translational corrections give an overall shift of the mass spectra of the baryons, the rotational corrections make the nucleon and Δ baryon states split. In the octet and decuplet representations, the linear m_s corrections take charge of splitting hyperon states. In this work, while we neglect the $1/N_c$ corrections,[1] we aim at scrutinizing the effects of the m_s corrections on the GFFs and the EMT distributions of the baryon octet. In the following subsection, we will exhibit the m_s corrections to the EMT distributions of the baryon octet.

TABLE I. Masses of the baryon octet.

Baryon	$M_{\rm sol}$ [MeV]	m_s correction [MeV]	m_B [MeV]
N	1256	95	1351
Λ	1256	122	1378
Σ	1256	149	1405
Ξ	1256	162	1418

A. Energy density

We start with examining the energy density $\varepsilon^B(r)$. It comes from the temporal component of the EMT density $T^{00}_{\mathrm{BF},B}$ defined as the Fourier transform of the mass form factor (11). If we integrate $\varepsilon^B(r)$ for a octet baryon over the 3D space, then we obtain the mass of the corresponding baryon

$$\begin{aligned}\int d^3r\varepsilon^B(r) &= \int d^3r\left(\mathcal{E}(r) + \left[M_1 + \frac{1}{\sqrt{3}}M_8\langle D_{88}\rangle_B\right][\mathcal{S}(r) - 2\mathcal{C}(r)]\right),\\ &= M_{\rm sol} + \left[M_1 + \frac{1}{\sqrt{3}}M_8\langle D_{88}\rangle_B\right]\frac{\Sigma_{\pi N}}{\bar{m}} \coloneqq m_B,\end{aligned} \tag{63}$$

with

$$\int d^3r\mathcal{E}(r) = M_{\rm sol}, \qquad \int d^3r\mathcal{S}(r) = \frac{\Sigma_{\pi N}}{\bar{m}},$$
$$\int d^3r\mathcal{C}(r) = 0. \tag{64}$$

Equation (63) coincides with the expression for the collective Hamiltonian (53). The form factor $A^B(t)$ is naturally normalized as

$$A^B(0) = \frac{1}{m_B}\int d^3r\varepsilon^B(r) = 1. \tag{65}$$

We list the values of the octet baryon masses in Table I. We find an obvious fact that the mass of the baryon becomes larger as the number of the strange quark in the valence level increases. One may wonder why the nucleon and hyperon masses are deviated from the experimental data. First, the classical soliton mass is typically overestimated at around ~300 MeV. Its origin may be understood as translational zero-mode corrections [126] and mesonic $1/N_c$ corrections. Second, the mass splittings of the hyperons are not described well without the m_s contributions mixed with the rotational ones, i.e., $\mathcal{O}(N_c^0, m_s)$. Introducing this mixed contribution [70,127], one can describe the mass splitting of the SU(3) baryons very well. In the current work, however, since we consider the baryon masses by using the mass form factors, it is technically very complicated to take into account such corrections. One may encounter triple sums of the quark states. Thus, we restrict ourselves to examine how the explicit flavor SU(3) symmetry breaking affects the EMT distribution and stability conditions.

In the upper-left and -right panels of Fig. 1, we show the 3D mass distributions and r^2-weighted ones of the baryon octet. The magnitude of the mass distribution over r becomes larger as the strangeness increases, which indicates that the mass of the corresponding octet baryon also becomes larger with the strangeness increased. Interestingly, as the mass of the baryon grows, the shape of the distribution gets more closely packed. This implies that the size of a heavier particle becomes more compact. We will observe this fact soon. In the IMF, we draw the corresponding 2D distributions in the middle-left and -right panels of Fig. 1 by implementing the IMF Abel transform (28). We find that the 2D mass distributions get closer to the origin of the position space, compared with the 3D ones. In the lower panel of Fig. 1, one can clearly see a narrower 2D distribution for the nucleon as a representative of the baryon octet. To quantify how strongly the mass distributions stretch out over position space, we introduce both the 2D and 3D mass radii in Eqs. (13) and (30), respectively. They are found to be

[1]Since the N_c leading contribution to the spin distribution arises from the $1/N_c$ rotational corrections, we take into account these corrections only for the spin distribution.

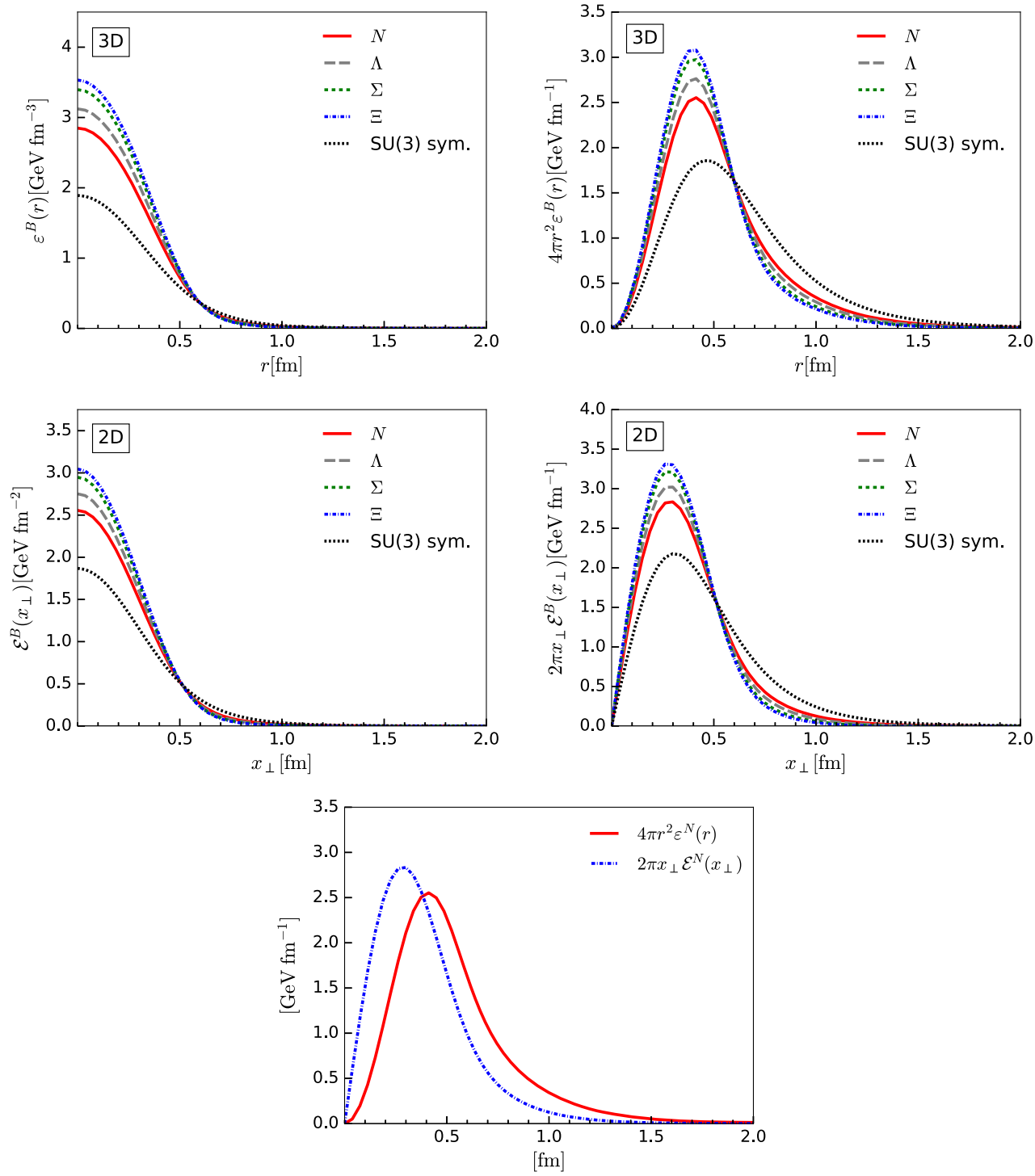

FIG. 1. 3D BF and 2D IMF mass distributions (upper- and middle-left panels) and r^2-weighted ones (upper- and middle-left panels) of the baryon octet and the classical nucleon, and comparison (lower panel) between the 3D BF and 2D IMF ones of the nucleon. The solid (red), long-dashed (gray), short-dashed (green), dashed-dotted (blue), and dotted (black) curves denote $\varepsilon^B(r)$ for the N, Λ, Σ, Ξ, and classical nucleon, respectively.

TABLE II. Various observables for the baryon octet and the nucleon with the SU(3) symmetry in the 3D BF: energy densities at the center $\epsilon^B(0)$; mean square radii $\langle r^2_\varepsilon\rangle_B$ and $\langle r^2_{\rm mech}\rangle_B$; normalized total angular momentum $2J^B(0)$; orbital angular momentum $2L^B$; isosinglet axial charge $g_A^{0,B}$; pressure densities $p^B(0)$ at the center of each baryon; nodal point of the pressure distribution $(r_0)_B$; D term $D(0)$.

B	$\epsilon^B(0)$ GeV/fm^3	$\langle r^2_\varepsilon\rangle_B$ fm^2	$2J^B(0)$	$g_A^{0,B}$	$2L^B$	$p^B(0)$ GeV/fm^3	$(r_0)_B$ fm	$D^B(0)$	$\langle r^2_{\rm mech}\rangle_B$ fm^2
N	2.85	0.31	1.00	0.48	0.52	0.42	0.56	−2.84	0.52
Λ	3.12	0.26	1.00	0.40	0.60	0.44	0.56	−2.91	0.51
Σ	3.40	0.20	1.00	0.53	0.47	0.45	0.55	−2.98	0.50
Ξ	3.53	0.17	1.00	0.38	0.62	0.46	0.55	−3.01	0.49
SU(3) sym.	1.89	0.54	1.00	0.46	0.54	0.35	0.57	−2.60	0.55

$$\langle r^2_\varepsilon\rangle_N = 0.31\ [\text{fm}^2], \quad \langle r^2_\varepsilon\rangle_\Lambda = 0.26\ [\text{fm}^2],$$
$$\langle r^2_\varepsilon\rangle_\Sigma = 0.20\ [\text{fm}^2], \quad \langle r^2_\varepsilon\rangle_\Xi = 0.17\ [\text{fm}^2],$$
$$\langle x^2_{\perp\mathcal{E}}\rangle_N = 0.15\ [\text{fm}^2], \quad \langle x^2_{\perp\mathcal{E}}\rangle_\Lambda = 0.11\ [\text{fm}^2],$$
$$\langle x^2_{\perp\mathcal{E}}\rangle_\Sigma = 0.07\ [\text{fm}^2], \quad \langle x^2_{\perp\mathcal{E}}\rangle_\Xi = 0.06\ [\text{fm}^2]. \tag{66}$$

As mentioned above, the heavier hyperons are more compact than the lighter ones:

$$\langle r^2_\varepsilon\rangle_N > \langle r^2_\varepsilon\rangle_\Lambda > \langle r^2_\varepsilon\rangle_\Sigma > \langle r^2_\varepsilon\rangle_\Xi,$$
$$\langle x^2_{\perp\mathcal{E}}\rangle_N > \langle x^2_{\perp\mathcal{E}}\rangle_\Lambda > \langle x^2_{\perp\mathcal{E}}\rangle_\Sigma > \langle x^2_{\perp\mathcal{E}}\rangle_\Xi. \tag{67}$$

Thus, we draw an important conclusion that the heavier octet baryon is energetically more compact in both the 3D BF and the 2D IMF. Thus, this is not changed by the IMF Abel transformation. Interestingly, including the m_s corrections to the mass distributions results in the energetically more compact nucleon and yields a larger value at the center of the distribution, compared to the classical nucleon (see Tables II and III).

B. Angular momentum density

Before we discuss the numerical results for the angular momentum density, we want to remark on the total angular momentum in the χQSM. In principle, the total angular momentum consists of the orbital angular momentum and spin of the quarks and gluons. In the χQSM, however, the gluonic degrees of freedom are absent or integrated out through the instanton vacuum. It implies that the baryon spin arises only from the orbital angular momentum and spin of the quarks and antiquarks. The intrinsic quark spin contribution or the singlet axial charge (g_A^0) can be obtained from the experimental data on the structure function g_1 extracted from the experimental data on polarized deep inelastic scattering. In a series of polarized deep inelastic scattering experiments, the quarks carry a small fraction of the nucleon spin, i.e., $g_A^0 \sim 0.33$ [9]. It leads one to posit that the orbital angular momentum of the quarks and gluons, and the spin of the gluon may have considerable contributions to the nucleon spin. The future EIC project may shed light on the spin structure of the nucleon. In the χQSM, we can explicitly decompose the intrinsic spin and orbital angular momentum of the quarks. The singlet axial charge was already studied in this model and found to be $g_A^0 \sim 0.44$ [70,128]. In this subsection, we will demonstrate that the missing part of the nucleon spin originates solely from the relativistic orbital motion of the quarks with the effects of the flavor SU(3) symmetry breakdown.

TABLE III. Various observables for the baryon octet and the nucleon with the SU(3) symmetry in the 2D IMF: energy densities at the center $\mathcal{E}^B(0)$; mean square radii $\langle x^2_{\perp\mathcal{E}}\rangle_B$ and $\langle x^2_{\perp\rm mech}\rangle_B$; pressure densities $\mathcal{P}^B(0)$ at the center of each baryon; nodal point of the pressure distribution $(x_{\perp 0})_B$.

B	$\mathcal{E}^B(0)$ GeV/fm^3	$\langle x^2_{\perp\mathcal{E}}\rangle_B$ fm^2	$\mathcal{P}^B(0)$ GeV/fm^3	$(x_{\perp 0})_B$ fm	$\langle x^2_{\perp\rm mech}\rangle_B$ fm^2
N	2.56	0.15	0.082	0.46	0.35
Λ	2.75	0.11	0.085	0.46	0.34
Σ	2.95	0.07	0.088	0.46	0.33
Ξ	3.05	0.06	0.090	0.46	0.33
SU(3) sym.	1.87	0.30	0.071	0.47	0.37

The spin density $\rho_J^B(r)$ arises from the mixed component of the EMT current $T^{0i}_{{\rm BF},B}$, and is normalized as the spin of a octet baryon:

$$J^B(0) = \int d^3r \rho_J^B(r) = \int d^3r \left(-\frac{1}{2I_1}\mathcal{I}_1(\boldsymbol{r}) + 2M_8\langle D_{83}\rangle_B \left[\frac{K_1}{I_1}\mathcal{I}_1(\boldsymbol{r}) - \mathcal{K}_1(\boldsymbol{r})\right]\right) = \frac{1}{2} \tag{68}$$

with

$$\int d^3r \mathcal{I}_1(\boldsymbol{r}) = -I_1, \qquad \int d^3r \mathcal{K}_1(\boldsymbol{r}) = -K_1. \tag{69}$$

If we integrate the angular momentum distributions of the octet baryon over 3D space, then we obtain the corresponding spin 1/2 (see Table II). As we explained already, one of the interesting results in the χQSM is that the total angular momentum can be decomposed into the orbital angular momentum and spin carried by quarks as follows:

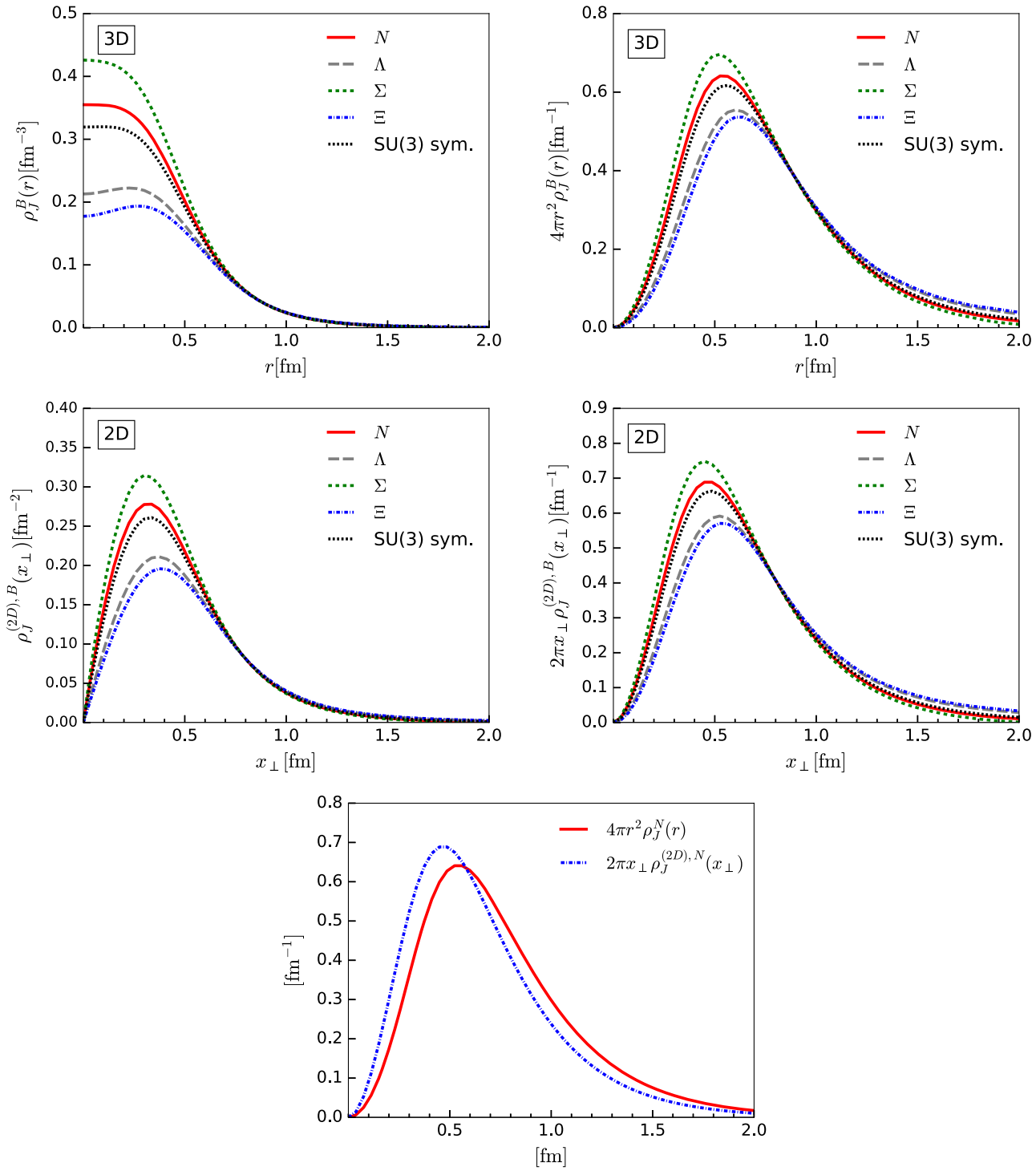

FIG. 2. 3D BF and 2D IMF total angular momentum distributions (upper- and middle-left panels) and r^2-weighted ones (upper- and middle-right panels) of the baryon octet and the nucleon with the flavor SU(3) symmetry, and comparison (lower panel) between the 3D BF and 2D IMF ones of the nucleon. The notations are the same as in Fig. 1.

$$J^B(0) = L^B + \frac{1}{2}g_A^{0,B}. \tag{70}$$

The explicit proof is provided in Appendix B. Using Eq. (70), we can separately define the orbital angular momentum and spin distributions. We first depict the total angular momentum distributions and r^2-weighted ones in the 3D BF for the baryon octet in the upper-left and -right panels of Fig. 2, respectively. The distributions of the baryon octet are split up with respect to that with the flavor

SU(3) symmetry. While the strengths of the distributions are enhanced for the nucleon and Σ baryon, those for the Ξ and Λ baryons are diminished. However, the normalizations of the distributions are not changed at all. In Table II, we list the properly normalized values of the $J^B(0)$ for the baryon octet. In the middle-left, middle-right, and lower panels of Fig. 2, we also present the same distributions in the 2D IMF. Similar to the 2D mass distributions, the 2D IMF angular momentum distributions are generically tilted inward, compared to the 3D BF distribution.

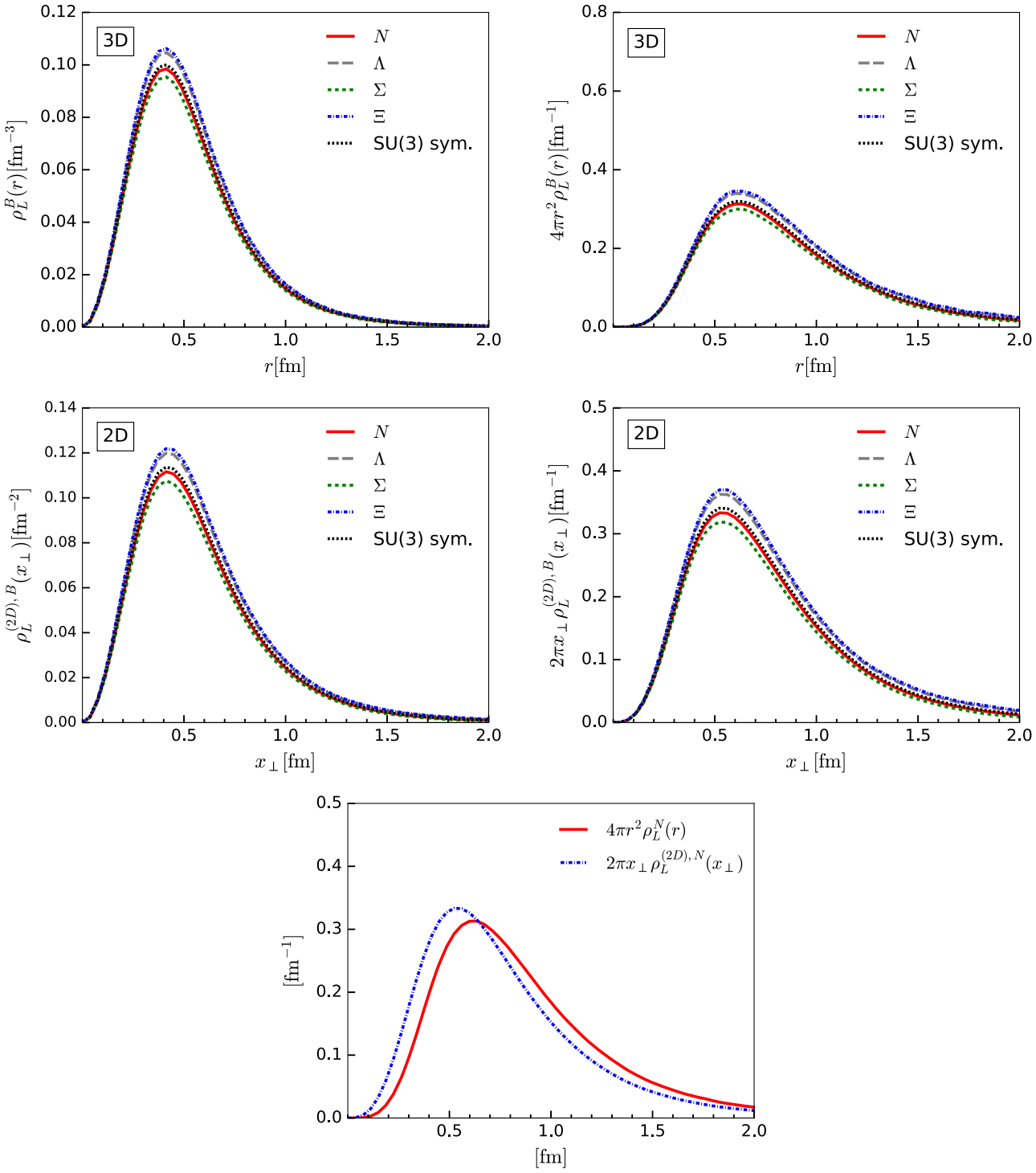

FIG. 3. 3D BF and 2D IMF orbital angular momentum distributions (upper- and middle-left panels) and r^2-weighted ones (upper- and middle-right panels) of the baryon octet and the nucleon with the flavor SU(3) symmetry, and comparison (lower panel) between the 3D BF and 2D IMF ones of the nucleon. The notations are the same as in Fig. 1.

As defined in Appendix B, the total angular momentum distribution is divided into the orbital angular momentum ρ_L^B and spin ρ_S^B distributions, and we draw them for both the 3D BF and the 2D IMF in Figs. 3 and 4, respectively. Integrating the distributions over 3D space yields

$$\int d^3r\rho_L^B(r) = L^B, \qquad \int d^3r\rho_S^B(r) = \frac{1}{2}g_A^{0,B}. \tag{71}$$

The separate values of the L^B and $g_A^{0,B}$ are listed in Table II. The fractions of the orbital angular momentum and spin

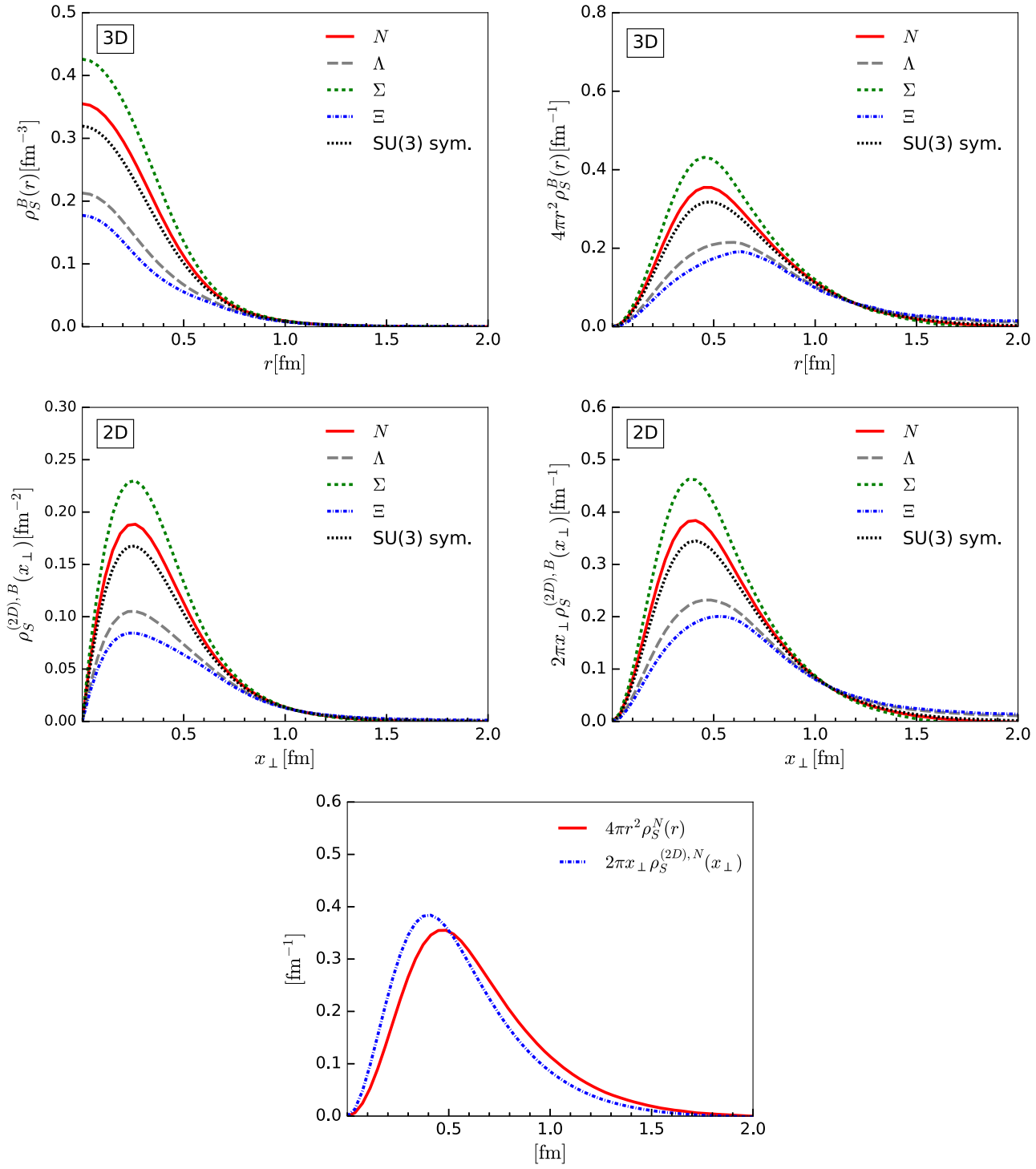

FIG. 4. 3D BF and 2D IMF spin distributions (upper- and middle-left panels) and r^2-weighted ones (upper- and middle-right panels) of the baryon octet and the nucleon with the flavor SU(3) symmetry, and comparison (lower panel) between the 3D BF and 2D IMF ones of the nucleon. The notations are the same as in Fig. 1.

carried by quarks inside the baryon are estimated to be around ∼50%, respectively, and they are well balanced. Though the relativistic effects on the baryon spin $J^B(0)$ for the nucleon and Σ baryon are slightly weaker than for the Λ and Ξ baryons, the orbital angular momentum is still very important in understanding the missing contribution to the baryon spin. The spin distributions are solely responsible for the nonzero values at the center of the angular momentum distributions, and the orbital angular momentum contributions dominate over the spin ones at the outer part. It means that the orbital angular momentum governs the outer part of the ρ_J^B. From those facts, one may expect that the ordering of the values of the ρ_J^B at the center is related to the ordering of the axial charges of the baryon octet (see Table II). Note that the axial charges of the baryon octet from the matrix element of the EMT current coincide with those from the matrix element of the axial-vector current [70,128,129].

C. Mechanical properties and stability conditions

We are now in a position to discuss the pressure and shear force distributions. Before we present the numerical results for these distributions, we want to mention how we acquire the stability conditions in the χQSM. In the current work, we treat $1/N_c$ and m_s corrections perturbatively. In the leading N_c approximation, the pressure $p(r)$ naturally satisfies the von Laue condition that is equivalent to the equation of motion [85]. However, once we introduce the next-to-leading-order contribution (say, m_s corrections) to $p(r)$, it breaks the von Laue condition. To remedy this problem, two different methods can be employed. The one is to minimize the baryon mass after quantizing the soliton, the so-called variation after quantization method. However, this method does not respect chiral symmetry in the large r region [130]. Thus, instead of using this method, we introduce the "quantization after variation" method. We first minimize the soliton mass and then quantize the soliton. So, the rotational corrections are considered as a small perturbation. Of course, we also have to pay the price in this case: the von Laue stability condition will again be broken. However, we can circumvent this problem by calculating the shear force distribution to avoid the violation of the stability condition instead of computing the pressure directly. We then reconstruct the pressure distribution from the obtained shear force distribution by solving the differential equation (20). Then, both the pressure and shear-force distributions comply with the global stability condition [119,122].

Yet another ambiguous point appears at large r. The chiral properties at large r are significant in the description of the GFFs, especially the D-term form factor. In the leading N_c contribution, it was well studied in Refs. [85,118,122] and agrees analytically with the results from chiral perturbation theory. However, in the present work, this chiral property is numerically spoiled by the finite box effects. We thus extrapolate the distribution at large r by adopting the pion Yukawa tail [122]. At the same time, once we take into account the next-to-leading order of m_s or $1/N_c$ corrections, this chiral property is broken again. However, since we treat them perturbatively, the next-to-leading-order corrections weakly contribute to the distributions at any value of r. Indeed we find that the m_s correction to the shear force distribution over r is less than 50% of the leading contribution. At the large r, this correction is saturated to 20% of the leading contribution. Thus, we are able to safely approximate shear force distribution at large r by using the pion tail used in the leading N_c contribution.

The reconstructed pressure distribution obviously satisfies the von Laue stability condition:

$$\int dr r^2 p(r) = 0. \tag{72}$$

In Fig. 5, we present the pressure distributions of the baryon octet in both the 3D BF and the 2D IMF, which are reconstructed from the shear force distributions. The comparison tells us that the size of the heavier octet baryon is mechanically more compact than that of the lighter octet baryon, as in the case of the mass distributions. It can be clearly seen by introducing the $(r_0)_B$ and $(x_{\perp 0})_B$ at which the pressure distribution vanishes for 3D BF and 2D IMF ones, respectively. Note that, to comply with the von Laue condition, this nodal point is necessary. As shown in the right panel of Fig. 5, the inner and outer parts are explicitly canceled out, so that the von Laue condition is satisfied. We find the following ordering for both the 3D BF and the 2D IMF:

$$\begin{aligned} &(r_0)_N < (r_0)_\Lambda < (r_0)_\Sigma < (r_0)_\Xi, \\ &(x_{\perp 0})_N < (x_{\perp 0})_\Lambda < (x_{\perp 0})_\Sigma < (x_{\perp 0})_\Xi. \end{aligned} \tag{73}$$

Indeed, the heavier octet baryon is a more compact object than the lighter one. We also find that for the heavier octet baryon the pressures for both the 3D BF and the 2D IMF at the core part are larger than the lighter ones (see Tables II and III).

In Fig. 6, we draw the shear-force distributions of the baryon octet in the 3D BF and the 2D IMF. We find that they are always positive over r. We can deduce from the fact that the 3D normal force is also positive for all values of r [see Eq. (20)]:

$$\frac{2}{3} s^B(r) + p^B(r) > 0, \qquad s^B(r) > 0. \tag{74}$$

It implies that the 2D one should also be positive over r:

$$\frac{1}{2} \mathcal{S}^B(x_\perp) + \mathcal{P}^B(x_\perp) > 0, \qquad \mathcal{S}^B(x_\perp) > 0. \tag{75}$$

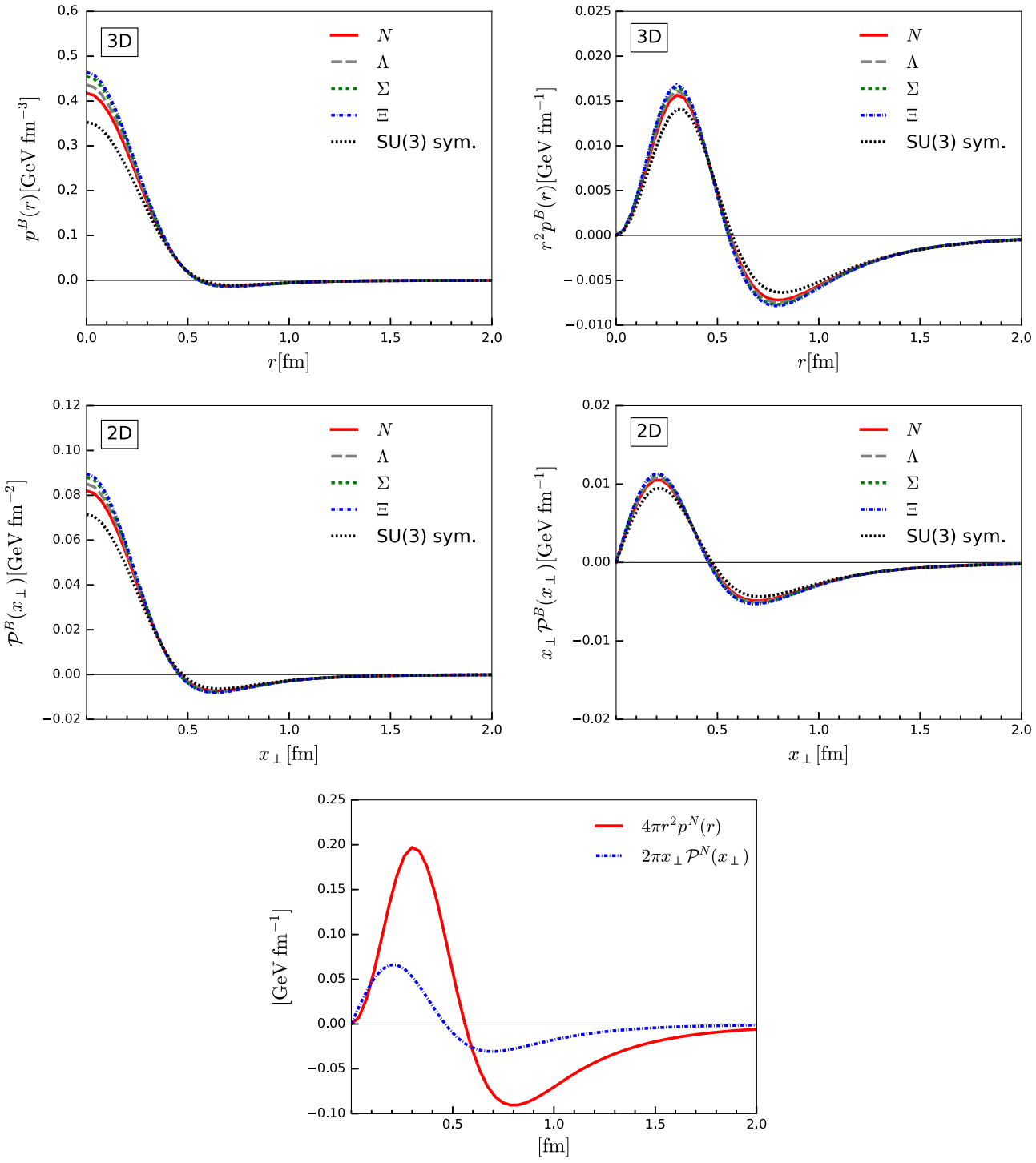

FIG. 5. 3D BF and 2D IMF pressure distributions (upper- and middle-left panels) and r^2-weighted ones (upper- and middle-right panels) of the baryon octet and the nucleon with the flavor SU(3) symmetry, and comparison (lower panel) between the 3D BF and 2D IMF ones of the nucleon. The notations are the same as in Fig. 1.

This positive shear-force distribution, $s^B(r) > 0$ or $\mathcal{S}^B(x_\perp) > 0$, is the signature of the negative D-term form factor at the zero momentum transfer. In Fig. 7, we also present the 3D BF and 2D IMF normal force distributions as a function of r for the baryon octet. They indeed satisfy the positivity over r. By integrating either r^2-weighted pressure or shear-force distributions, one can obtain the D terms. The numerical results for the D terms of the baryon octet are derived as

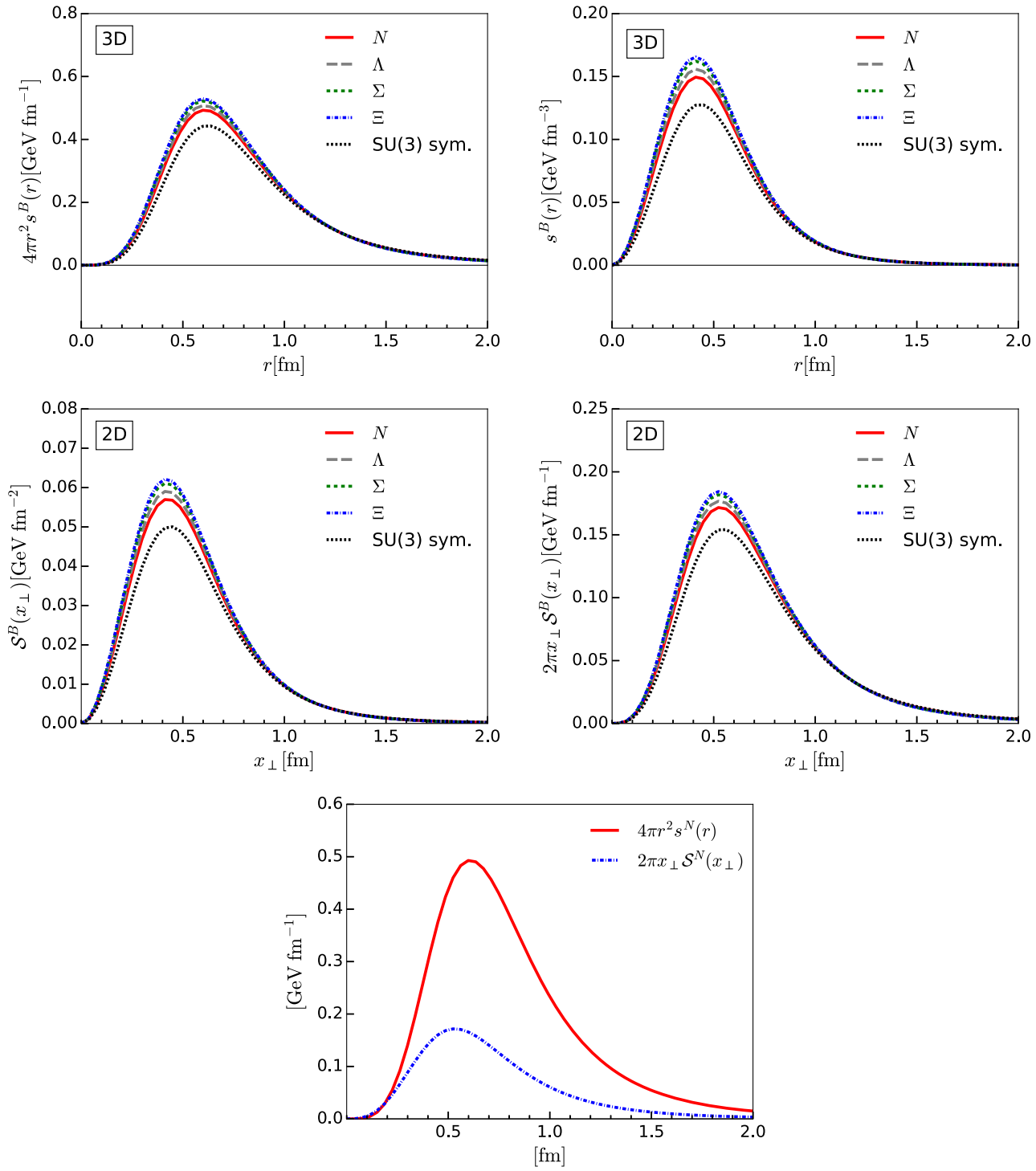

FIG. 6. 3D BF and 2D IMF shear-force distributions (upper- and middle-left panels) and r^2-weighted ones (upper- and middle-right panels) of the baryon octet and the nucleon with the flavor SU(3) symmetry, and comparison (lower panel) between the 3D BF and 2D IMF ones of the nucleon. The notations are the same as in Fig. 1.

$$D^N(0) = -2.84, \qquad D^\Lambda(0) = -2.91,$$
$$D^\Sigma(0) = -2.98, \qquad D^\Xi(0) = -3.01. \tag{76}$$

As expected, we obtain the negative D terms for the baryon octet. Interestingly, we find that the heavier octet baryon has a larger value of the D term. To quantify the mechanical size of the octet baryon, we estimate the 3D BF and 2D IMF mechanical radii of the baryon octet as follows:

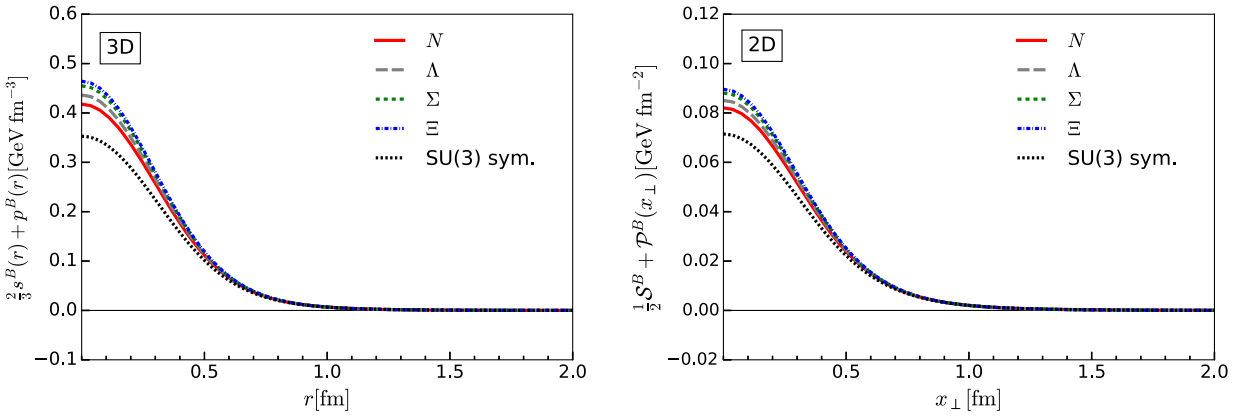

FIG. 7. 3D BF and 2D IMF normal force distributions of the baryon octet and the nucleon with the flavor SU(3) symmetry. The notations are the same as in Fig. 1.

$$\langle r^2_{\rm mech}\rangle_N = 0.52\ [\mathrm{fm}^2], \quad \langle r^2_{\rm mech}\rangle_\Lambda = 0.51\ [\mathrm{fm}^2],$$
$$\langle r^2_{\rm mech}\rangle_\Sigma = 0.50\ [\mathrm{fm}^2], \quad \langle r^2_{\rm mech}\rangle_\Xi = 0.49\ [\mathrm{fm}^2],$$
$$\langle x^2_{\perp{\rm mech}N} = 0.36\ [\mathrm{fm}^2], \quad \langle x^2_{\perp{\rm mech}}\rangle_\Lambda = 0.35\ [\mathrm{fm}^2],$$
$$\langle x^2_{\perp{\rm mech}}\rangle_\Sigma = 0.35\ [\mathrm{fm}^2], \quad \langle x^2_{\perp{\rm mech}}\rangle_\Xi = 0.35\ [\mathrm{fm}^2]. \quad (77)$$

This indicates that the heavier octet baryon is mechanically a more compact object than the lighter one. Since, however, the m_s corrections to the mechanical radii are negligible, the mechanical sizes of octet baryons are rather comparable. All the relevant physical observables are listed in Tables II and III. Last but not least, it is of great interest to see the ordering of the magnitude of the nucleon radii with the flavor SU(3) symmetry breaking. We observe the following ordering:

$$\langle r^2_{\mathcal{E}}\rangle_N < \langle r^2_{\rm mech}\rangle_N < \langle r^2_{\rm charge}\rangle_N, \quad (78)$$

where $\langle r^2_{\rm charge}\rangle_N$ is the charge radius of the nucleon taken from Ref. [70]. We find that the ordering of the radii are kept to be the same as the results with flavor SU(3) symmetry for both the 3D BF and the 2D IMF.

D. Results for the gravitational form factors

The GFFs are obtained by the Fourier transform of the corresponding EMT distributions. In Fig. 8, we present the numerical results for the GFFs of the baryon octet as functions of the momentum transfer t. In the upper left panel of Fig. 8, the results of the $A^B(t)$ show that the form factor of the heavier octet baryon falls off slowly in comparison with that of the lighter one. It reflects the fact that the heavier octet baryon is energetically more compact than the lighter one. A similar feature was found in the case of mass distribution of the heavy baryon [88]. In the upper right panel of Fig. 8, the results of the $J^B(t)$ show somewhat different features as observed in the angular momentum distribution in the previous subsection. The form factor $J^B(t)$ for the nucleon and Σ baryon falls off slowly in comparison with those for the Ξ and Λ baryons. Lastly, in the lower panel of Fig. 8, the D-term form factors are drawn. The negativity of the D term for the octet baryon can be also deduced from the positive shear-force distributions over r. Thus, the negative D term is connected to the positivity of the normal force distribution. We find that the heavier octet baryon possesses the larger absolute value of the D term. The mechanical radius can be also obtained from the D-term form factor, but unlike a typical form factor, the slope of the D-term form factor does not give the mechanical radius of a baryon. Interestingly, the mechanical radii have opposite behavior compared to the D term. The heavier octet baryon possesses a smaller size of mechanical radius than the lighter one.

VI. SUMMARY AND OUTLOOK

In the present work, we aimed at investigating the gravitational form factors of the baryon octet and the corresponding energy-momentum tensor distributions within the SU(3) chiral quark-soliton model, considering the effects of flavor SU(3) symmetry breaking. Starting from the matrix element of the energy-momentum tensor current for the baryon octet, we were able to compute the four different densities: mass, angular momentum, pressure, and shear force in both the 3D Breit and 2D infinite momentum frames. Integrating the energy density over position space yielded the masses of the baryon octet, so that the mass form factor was properly normalized to be $A^B(0) = 1$. We also found that, with the flavor SU(3) symmetry breaking, the mass radius of the heavier octet baryon is larger than that of the lighter one. It implies that the heavier octet baryon is energetically a more compact object, compared with the lighter one. We then examined the angular momentum densities of the octet baryons. Integrating the angular momentum densities over position space gave the spins of the baryon octet even in the flavor SU(3) symmetry broken case, so that the spin form factors

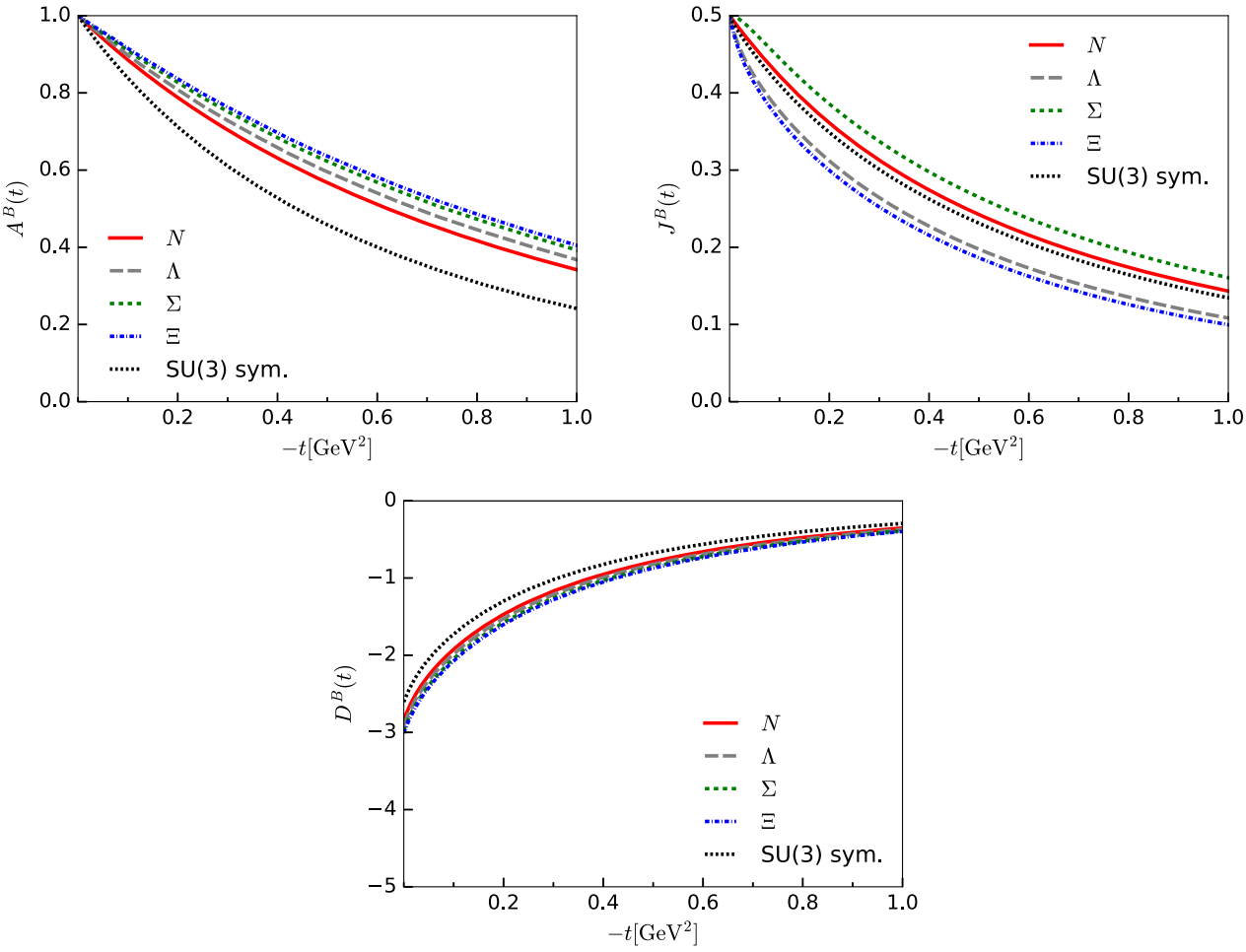

FIG. 8. Results for the EMT form factors $A^B(t)$, $D^B(t)$, and $J^B(t)$ of the baryon octet and the nucleon with the flavor SU(3) symmetry. The solid (red), long-dashed (gray), short-dashed (green), dashed-dotted (blue), and dotted (black) curves denote $s^B(r)$ for the N, Λ, Σ, Ξ, and nucleon with the flavor SU(3) symmetry, respectively. The notations are the same as in Fig. 1.

were properly normalized to be $J^B(0) = 1/2$. Interestingly, the total angular momentum was decomposed into the flavor-singlet axial charge and orbital angular momentum $J^B = L^B + g_A^{0,B}/2$. The quark spin contributions to the angular momentum of the octet baryon were estimated at around 50%. Since there are no gluonic degrees of freedom in the chiral quark-soliton model, the missing contributions were solely explained by the orbital motion of the quarks. While the m_s corrections differently contribute to the angular momentum distributions for the octet baryons, their effects were rather mild. So, both the spin and the orbital angular momentum contributions to the angular momentum distributions for the octet baryons are well balanced overall. Lastly, we computed the shear-force distribution from the model calculation and then reconstructed the pressure distribution from the shear-force distribution by using the equilibrium differential equation. In addition, we extrapolated the shear-force distribution at large r to remove the numerical redundancy by tagging the pion Yukawa tail. So, the pressure obviously complied with the von Laue condition. One of the remarkable results observed in this work is that the shear force is always positive for any values of the r. It indicates the positive normal force over r and the negative D term. It means that the local stability condition is still preserved even if we take into account the effects of the flavor SU(3) symmetry breaking. We also estimated the D terms for the octet baryons and found that the heavier octet baryon has a larger absolute value of the D term than the lighter one. On the other hand, the mechanical radius of the heavier octet baryon was smaller than that of the lighter one. It implies that the heavier octet baryon is mechanically a more compact object than the lighter one. We presented the numerical results for the gravitational form factors of the baryon octet as functions of the momentum transfer t by the Fourier transform of the given energy-momentum tensor distributions. The mass and angular momentum form factor $A^B(t)$ and $J^B(t)$ were properly normalized to 1 and $1/2$, respectively, their slopes reflect the values of the distribution

radius. When it comes to the D-term form factors, as expected, their negative values were obtained. In addition, m_s corrections to the D terms were found to be rather small.

ACKNOWLEDGMENTS

The work was supported by the Basic Science Research Program through the National Research Foundation of Korea funded by the Korean government (Ministry of Education, Science and Technology, MEST), Grants No. 2021R1A2C2093368 and No. 2018R1A5A1025563.

APPENDIX A: DENSITIES AND REGULARIZATION FUNCTIONS

In this section, we collect the explicit expressions for the EMT distributions. The mass distribution is written as

$$\begin{aligned}
\frac{1}{N_c}\mathcal{E}(\boldsymbol{r}) &= E_v\psi_v^\dagger(\boldsymbol{r})\psi_v(\boldsymbol{r}) + \sum_{n=\text{all}}\psi_n^\dagger(\boldsymbol{r})\psi_n(\boldsymbol{r})R_0(E_n),\\
\frac{1}{N_c}\mathcal{S}(\boldsymbol{r}) &= \psi_v^\dagger(\boldsymbol{r})\gamma^0\psi_v(\boldsymbol{r}) + \sum_{n=\text{all}}\psi_n^\dagger(\boldsymbol{r})\gamma^0\psi_n(\boldsymbol{r})R_1(E_n),\\
\frac{1}{N_c}\mathcal{C}(\boldsymbol{r}) &= \frac{1}{2}\sum_{n\neq v}\frac{E_n+E_v}{E_n-E_v}\langle n|\gamma^0|v\rangle\psi_v^\dagger(\boldsymbol{r})\psi_n(\boldsymbol{r}) + \frac{1}{4}\sum_{\substack{n=\text{all}\\m=\text{all}}}(E_n+E_m)\langle n|\gamma^0|m\rangle\psi_m^\dagger(\boldsymbol{r})\psi_n(\boldsymbol{r})R_5(E_n,E_m),
\end{aligned} \tag{A1}$$

and the angular momentum distribution is given by

$$\begin{aligned}
\frac{1}{N_c}\mathcal{I}_1(\boldsymbol{r}) &= \sum_{n\neq v}\frac{1}{E_n-E_v}\langle n|\tau_3|v\rangle\psi_v^\dagger(\boldsymbol{r})\hat{J}_3\psi_n(\boldsymbol{r}) + \frac{1}{2}\sum_{\substack{n=\text{all}\\m=\text{all}}}\langle n|\tau_3|m\rangle\psi_m^\dagger(\boldsymbol{r})\hat{J}_3\psi_n(\boldsymbol{r})R_3(E_n,E_m),\\
\frac{1}{N_c}\mathcal{K}_1(\boldsymbol{r}) &= \sum_{n\neq v}\frac{1}{E_n-E_v}\langle n|\gamma^0\tau_3|v\rangle\psi_v^\dagger(\boldsymbol{r})\hat{J}_3\psi_n(\boldsymbol{r}) + \frac{1}{2}\sum_{\substack{n=\text{all}\\m=\text{all}}}\langle n|\gamma^0\tau_3|m\rangle\psi_m^\dagger(\boldsymbol{r})\hat{J}_3\psi_n(\boldsymbol{r})R_5(E_n,E_m).
\end{aligned} \tag{A2}$$

The shear-force distributions are expressed as

$$\begin{aligned}
\frac{1}{N_c}\mathcal{N}_1(\boldsymbol{r}) &= \frac{3}{2}\left[\psi_v^\dagger(\boldsymbol{r})\left(\gamma^0(\hat{\boldsymbol{n}}\cdot\boldsymbol{\gamma})(\hat{\boldsymbol{n}}\cdot\boldsymbol{p}) - \frac{1}{3}\gamma^0(\boldsymbol{\gamma}\cdot\boldsymbol{p})\right)\psi_v(\boldsymbol{r}) + \sum_{n=\text{all}}\psi_n^\dagger(\boldsymbol{r})\left(\gamma^0(\hat{\boldsymbol{n}}\cdot\boldsymbol{\gamma})(\hat{\boldsymbol{n}}\cdot\boldsymbol{p}) - \frac{1}{3}\gamma^0(\boldsymbol{\gamma}\cdot\boldsymbol{p})\right)\psi_n(\boldsymbol{r})R_1(E_n)\right],\\
\frac{1}{N_c}\mathcal{N}_2(\boldsymbol{r}) &= \frac{3}{2}\left[\sum_{n\neq v}\frac{1}{E_n-E_v}\langle n|\gamma^0|v\rangle\psi_v^\dagger(\boldsymbol{r})\left(\gamma^0(\hat{\boldsymbol{n}}\cdot\boldsymbol{\gamma})(\hat{\boldsymbol{n}}\cdot\boldsymbol{p}) - \frac{1}{3}\gamma^0(\boldsymbol{\gamma}\cdot\boldsymbol{p})\right)\psi_n(\boldsymbol{r})\right.\\
&\quad\left. + \frac{1}{2}\sum_{\substack{n=\text{all}\\m=\text{all}}}\langle n|\gamma^0|m\rangle\psi_m^\dagger(\boldsymbol{r})\left(\gamma^0(\hat{\boldsymbol{n}}\cdot\boldsymbol{\gamma})(\hat{\boldsymbol{n}}\cdot\boldsymbol{p}) - \frac{1}{3}\gamma^0(\boldsymbol{\gamma}\cdot\boldsymbol{p})\right)\psi_n(\boldsymbol{r})R_2(E_n,E_m)\right],
\end{aligned} \tag{A3}$$

where the regularization functions are defined by

$$\begin{aligned}
R_0(E_n) &= \frac{1}{4\sqrt{\pi}}\int\frac{du}{u^{3/2}}\phi(u,\Lambda)e^{-uE_n^2},\\
R_1(E_n) &= -\frac{E_n}{2\sqrt{\pi}}\int\frac{du}{\sqrt{u}}\phi(u,\Lambda)e^{-uE_n^2},\\
R_2(E_n,E_m) &= \frac{1}{2\sqrt{\pi}}\int\frac{du}{\sqrt{u}}\phi(u,\Lambda)\frac{E_ne^{-uE_n^2}-E_me^{-uE_m^2}}{E_n-E_m},\\
R_3(E_n,E_m) &= \frac{1}{2\sqrt{\pi}}\int\frac{du}{\sqrt{u}}\phi(u,\Lambda)\left[\frac{1}{u}\frac{e^{-uE_n^2}-e^{-uE_m^2}}{E_m^2-E_n^2} - \frac{E_ne^{-uE_n^2}+E_me^{-uE_m^2}}{E_n+E_m}\right],\\
R_5(E_n,E_m) &= \frac{1}{2}\frac{\text{sign}(E_n)-\text{sign}(E_m)}{E_n-E_m},
\end{aligned} \tag{A4}$$

with $\psi_v(\boldsymbol{r}) \coloneqq \langle \boldsymbol{r}|v\rangle$, $\psi_n(\boldsymbol{r}) \coloneqq \langle \boldsymbol{r}|n\rangle$ and $\hat{J}_3 = \hat{L}_3 + \hat{S}_3$. $|v\rangle$ and $|n\rangle$ denote the states of the valence and sea quarks with the corresponding eigenenergies E_v and E_n of the single-quark Hamiltonian $h(U)$, respectively. In addition, the dynamical parameters are defined as follows:

$$\begin{aligned}\frac{1}{N_c}I_1 &= \frac{1}{2}\left[\sum_{n\neq v}\frac{1}{E_n - E_v}\langle n|\tau_3|v\rangle\langle v|\tau_3|n\rangle + \frac{1}{2}\sum_{\substack{n=\text{all}\\ m=\text{all}}}\langle n|\tau_3|m\rangle\langle m|\tau_3|n\rangle R_3(E_n, E_m)\right],\\ \frac{1}{N_c}K_1 &= \frac{1}{2}\left[\sum_{n\neq v}\frac{1}{E_n - E_v}|n|\gamma^0\tau_3|v\rangle|v|\tau_3|n\rangle + \frac{1}{2}\sum_{\substack{n=\text{all}\\ m=\text{all}}}\langle n|\gamma^0\tau_3|m\rangle|m|\tau_3|n\rangle R_5(E_n, E_m)\right].\end{aligned} \tag{A5}$$

APPENDIX B: ANGULAR-MOMENTUM DECOMPOSITION

We show how the total angular momentum can be decomposed into the spin and orbital angular momentum contributions. It was derived in the SU(2) χQSM [85,131], and we generalize it in SU(3). The angular momentum distribution is obtained to be

$$\rho_J^B(\boldsymbol{r}) = -\frac{1}{2I_1}\mathcal{I}_1(\boldsymbol{r}) + 2M_8\langle D_{83}\rangle_B\left(\frac{K_1}{I_1}\mathcal{I}_1(\boldsymbol{r}) - \mathcal{K}_1(\boldsymbol{r})\right), \tag{B1}$$

where each density is given by

$$\begin{aligned}\mathcal{I}_1(\boldsymbol{r}) &= \frac{N_c}{4}\left[\sum_{n\neq v}\frac{1}{E_n - E_v}\langle n|\tau_3|v\rangle\psi_v^\dagger(\boldsymbol{r})(2\hat{L}_3 + (E_n + E_m)\gamma_5(\hat{\boldsymbol{r}}\times\sigma)_3)\psi_n(\boldsymbol{r})\right.\\ &\quad\left. + \frac{1}{2}\sum_{\substack{n=\text{all}\\ m=\text{all}}}\langle n|\tau_3|m\rangle\psi_m^\dagger(\boldsymbol{r})(2\hat{L}_3 + (E_n + E_m)\gamma_5(\hat{\boldsymbol{r}}\times\sigma)_3)\psi_n(\boldsymbol{r})R_3(E_n, E_m)\right],\\ \mathcal{K}_1(\boldsymbol{r}) &= \frac{N_c}{4}\left[\sum_{n\neq v}\frac{1}{E_n - E_v}\langle n|\gamma^0\tau_3|v\rangle\psi_v^\dagger(\boldsymbol{r})(2\hat{L}_3 + (E_n + E_m)\gamma_5(\hat{\boldsymbol{r}}\times\sigma)_3)\psi_n(\boldsymbol{r})\right.\\ &\quad\left. + \frac{1}{2}\sum_{\substack{n=\text{all}\\ m=\text{all}}}\langle n|\gamma^0\tau_3|m\rangle\psi_m^\dagger(\boldsymbol{r})(2\hat{L}_3 + (E_n + E_m)\gamma_5(\hat{\boldsymbol{r}}\times\sigma)_3)\psi_n(\boldsymbol{r})R_5(E_n, E_m)\right].\end{aligned} \tag{B2}$$

To avoid numerical error discussed in Ref. [129], we manipulate the given densities. The second terms of each density can be easily converted into the spin and orbital angular momentum operators as follows:

$$\psi_m^\dagger(\boldsymbol{r})((E_n + E_m)\gamma_5(\hat{\boldsymbol{r}}\times\sigma)_3)\psi_n(\boldsymbol{r}) = \varepsilon_{3jk}\psi_m^\dagger(\boldsymbol{r})\{H, \gamma_5\hat{\boldsymbol{r}}^j\sigma^k\}\psi_n(\boldsymbol{r}) = \psi_m^\dagger(\boldsymbol{r})(2\hat{L}_3 + 2\sigma_3)\psi_n(\boldsymbol{r}). \tag{B3}$$

After that we are able to rewrite the densities as follows:

$$\begin{aligned}\frac{1}{N_c}\mathcal{I}_1(\boldsymbol{r}) &= \sum_{n\neq v}\frac{1}{E_n - E_v}\langle n|\tau_3|v\rangle\psi_v^\dagger(\boldsymbol{r})\hat{J}_3\psi_n(\boldsymbol{r}) + \frac{1}{2}\sum_{\substack{n=\text{all}\\ m=\text{all}}}\langle n|\tau_3|m\rangle\psi_m^\dagger(\boldsymbol{r})\hat{J}_3\psi_n(\boldsymbol{r})R_3(E_n, E_m),\\ \frac{1}{N_c}\mathcal{K}_1(\boldsymbol{r}) &= \sum_{n\neq v}\frac{1}{E_n - E_v}\langle n|\gamma^0\tau_3|v\rangle\psi_v^\dagger(\boldsymbol{r})\hat{J}_3\psi_n(\boldsymbol{r}) + \frac{1}{2}\sum_{\substack{n=\text{all}\\ m=\text{all}}}\langle n|\gamma^0\tau_3|m\rangle\psi_m^\dagger(\boldsymbol{r})\hat{J}_3\psi_n(\boldsymbol{r})R_5(E_n, E_m),\end{aligned} \tag{B4}$$

where $\hat{J}_3 = \hat{L}_3 + \hat{S}_3$ and the spin operator $\hat{S}$ are defined as $\hat{S}_3 = \frac{1}{2}\sigma_3$. Thus, we can define the orbital and spin densities by replacing the total angular momentum operator $\hat{J}_3$ by either $\hat{L}_3$ or $\hat{S}_3$:

$$\rho_J^B(r) = \rho_L^B(r) + \rho_S^B(r). \tag{B5}$$

Here we are able to simplify Eq. (B4) by using the fact that the quark states are eigenstates of the grand spin operator ($\hat{G}_3 = \hat{J}_3 + \hat{T}_3$):

$$\frac{1}{N_c}\int d^3r\mathcal{I}_1(\boldsymbol{r}) = \sum_{n\neq v}\frac{1}{E_n - E_v}\langle n|\tau_3|v\rangle\langle v|(\hat{G}_3 - \hat{T}_3)|n\rangle + \frac{1}{2}\sum_{\substack{n=\text{all}\\ m=\text{all}}}\langle n|\tau_3|m\rangle\langle m|(\hat{G}_3 - \hat{T}_3)|n\rangle R_3(E_n, E_m),$$
$$\frac{1}{N_c}\int d^3r\mathcal{K}_1(\boldsymbol{r}) = \sum_{n\neq v}\frac{1}{E_n - E_v}\langle n|\gamma^0\tau_3|v\rangle\langle v|(\hat{G}_3 - \hat{T}_3)n + \frac{1}{2}\sum_{\substack{n=\text{all}\\ m=\text{all}}}\langle n|\gamma^0\tau_3|m\rangle\langle m|(\hat{G}_3 - \hat{T}_3)nR_5(E_n, E_m). \tag{B6}$$

Note that the matrix elements $\langle m|\hat{G}_3|n\rangle = G_3\delta_{mn}$ vanish for both densities. By integrating both sides over the 3D space, the densities $\mathcal{I}_1$ and $\mathcal{K}_1$ becomes the dynamical parameter I_1 and K_1 defined in Eq. (A5):

$$\int d^3r\mathcal{I}_1(\boldsymbol{r}) = -I_1, \qquad \int d^3r\mathcal{K}_1(\boldsymbol{r}) = -K_1. \tag{B7}$$

Therefore, the integration of the angular momentum density over the 3D space always gives the spin normalization

$$\int d^3r\rho_J^B(r) = \frac{1}{2}. \tag{B8}$$

[1] I. Y. Kobzarev and L. B. Okun, Zh. Eksp. Teor. Fiz. **43**, 1904 (1962).
[2] H. Pagels, Phys. Rev. **144**, 1250 (1966).
[3] V. D. Burkert, L. Elouadrhiri, and F. X. Girod, Nature (London) **557**, 396 (2018).
[4] K. Kumerički, Nature (London) **570**, E1 (2019).
[5] V. D. Burkert, L. Elouadrhiri, and F. X. Girod, arXiv:2104.02031.
[6] S. J. Brodsky *et al.*, Int. J. Mod. Phys. E **29**, 2030006 (2020).
[7] Kyungseon Joo and Stefan Diehl, $N \to \Delta$ Transition GPDs with CLAS12.
[8] J.-Y. Kim, Phys. Lett. B **834**, 137442 (2022).
[9] C. A. Aidala, S. D. Bass, D. Hasch, and G. K. Mallot, Rev. Mod. Phys. **85**, 655 (2013).
[10] S. D. Bass, Rev. Mod. Phys. **77**, 1257 (2005).
[11] I. Y. Kobsarev and V. I. Zakharov, Ann. Phys. (N.Y.) **60**, 448 (1970).
[12] K. L. Ng, Phys. Rev. D **47**, 5187 (1993).
[13] S. Cotogno, C. Lorcé, P. Lowdon, and M. Morales, Phys. Rev. D **101**, 056016 (2020).
[14] M. V. Polyakov and A. G. Shuvaev, arXiv:hep-ph/0207153.
[15] X.-D. Ji, W. Melnitchouk, and X. Song, Phys. Rev. D **56**, 5511 (1997).
[16] P. Schweitzer, S. Boffi, and M. Radici, Phys. Rev. D **66**, 114004 (2002).
[17] J.-H. Jung, U. Yakhshiev, and H.-C. Kim, J. Phys. G **41**, 055107 (2014).
[18] P. Hagler, J. W. Negele, D. B. Renner, W. Schroers, T. Lippert, and K. Schilling (LHPC, SESAM Collaborations), Phys. Rev. D **68**, 034505 (2003).
[19] M. Gockeler, R. Horsley, D. Pleiter, P. E. L. Rakow, A. Schafer, G. Schierholz, and W. Schroers (QCDSF Collaboration), Phys. Rev. Lett. **92**, 042002 (2004).
[20] B. Pasquini and S. Boffi, Phys. Lett. B **653**, 23 (2007).
[21] D. S. Hwang and D. Mueller, Phys. Lett. B **660**, 350 (2008).
[22] Z. Abidin and C. E. Carlson, Phys. Rev. D **77**, 115021 (2008).
[23] S. J. Brodsky and G. F. de Teramond, Phys. Rev. D **78**, 025032 (2008).
[24] B. Pasquini, M. V. Polyakov, and M. Vanderhaeghen, Phys. Lett. B **739**, 133 (2014).
[25] D. Chakrabarti, C. Mondal, and A. Mukherjee, Phys. Rev. D **91**, 114026 (2015).
[26] C. Lorcé, H. Moutarde, and A. P. Trawiński, Eur. Phys. J. C **79**, 89 (2019).
[27] O. V. Teryaev, Front. Phys. **11**, 111207 (2016).
[28] P. E. Shanahan and W. Detmold, Phys. Rev. Lett. **122**, 072003 (2019).
[29] P. E. Shanahan and W. Detmold, Phys. Rev. D **99**, 014511 (2019).
[30] M. J. Neubelt, A. Sampino, J. Hudson, K. Tezgin, and P. Schweitzer, Phys. Rev. D **101**, 034013 (2020).
[31] I. V. Anikin, Phys. Rev. D **99**, 094026 (2019).
[32] H. Alharazin, D. Djukanovic, J. Gegelia, and M. V. Polyakov, Phys. Rev. D **102**, 076023 (2020).
[33] J. Gegelia and M. V. Polyakov, Phys. Lett. B **820**, 136572 (2021).
[34] M. Varma and P. Schweitzer, Phys. Rev. D **102**, 014047 (2020).
[35] M. Fujita, Y. Hatta, S. Sugimoto, and T. Ueda, Prog. Theor. Exp. Phys. **2022**, 093B06 (2022).
[36] K. A. Mamo and I. Zahed, Phys. Rev. D **106**, 086004 (2022).
[37] D. A. Pefkou, D. C. Hackett, and P. E. Shanahan, Phys. Rev. D **105**, 054509 (2022).
[38] K. Azizi and U. Özdem, Eur. Phys. J. C **80**, 104 (2020).
[39] M. V. Polyakov and H.-D. Son, J. High Energy Phys. 09 (2018) 156.

[40] A. Freese and G. A. Miller, Phys. Rev. D **105**, 014003 (2022).
[41] A. Freese and G. A. Miller, Phys. Rev. D **104**, 014024 (2021).
[42] A. Freese and G. A. Miller, Phys. Rev. D **103**, 094023 (2021).
[43] M. V. Polyakov and A. Tandogan, Phys. Rev. D **101**, 118501 (2020).
[44] K. Azizi and U. Özdem, Nucl. Phys. **A1015**, 122296 (2021).
[45] U. Özdem and K. Azizi, Phys. Rev. D **101**, 054031 (2020).
[46] M. V. Polyakov and B.-D. Sun, Phys. Rev. D **100**, 036003 (2019).
[47] W. Cosyn, S. Cotogno, A. Freese, and C. Lorcé, Eur. Phys. J. C **79**, 476 (2019).
[48] J.-Y. Kim, B.-D. Sun, D. Fu, and H.-C. Kim, arXiv:2208.01240.
[49] A. Freese and W. Cosyn, arXiv:2207.10787 [Phys. Rev. D (to be published)].
[50] A. Freese and W. Cosyn, arXiv:2207.10788 [Phys. Rev. D (to be published)].
[51] A. Freese and I. C. Cloët, Phys. Rev. C **100**, 015201 (2019).
[52] B.-D. Sun and Y.-B. Dong, Phys. Rev. D **101**, 096008 (2020).
[53] E. Epelbaum, J. Gegelia, U. G. Meißner, and M. V. Polyakov, Phys. Rev. D **105**, 016018 (2022).
[54] D. Fu, B.-D. Sun, and Y. Dong, Phys. Rev. D **105**, 096002 (2022).
[55] H. Alharazin, E. Epelbaum, J. Gegelia, U. G. Meißner, and B. D. Sun, Eur. Phys. J. C **82**, 907 (2022).
[56] J. Y. Panteleeva and M. V. Polyakov, Phys. Lett. B **809**, 135707 (2020).
[57] U. Özdem and K. Azizi, Phys. Rev. D **101**, 114026 (2020).
[58] M. V. Polyakov, Phys. Lett. B **555**, 57 (2003).
[59] D. R. Yennie, M. M. Lévy, and D. G. Ravenhall, Rev. Mod. Phys. **29**, 144 (1957).
[60] M. Burkardt, Phys. Rev. D **62**, 071503 (2000); **66**, 119903 (E) (2002).
[61] M. Burkardt, Int. J. Mod. Phys. A **18**, 173 (2003).
[62] G. A. Miller, Phys. Rev. Lett. **99**, 112001 (2007).
[63] R. L. Jaffe, Phys. Rev. D **103**, 016017 (2021).
[64] J. Y. Panteleeva and M. V. Polyakov, Phys. Rev. D **104**, 014008 (2021).
[65] J.-Y. Kim and H.-C. Kim, Phys. Rev. D **104**, 074019 (2021).
[66] E. Epelbaum, J. Gegelia, N. Lange, U. G. Meißner, and M. V. Polyakov, Phys. Rev. Lett. **129**, 012001 (2022).
[67] J. Y. Panteleeva, E. Epelbaum, J. Gegelia, and U. G. Meißner, Phys. Rev. D **106**, 056019 (2022).
[68] D. Diakonov, V. Y. Petrov, and P. V. Pobylitsa, Nucl. Phys. **B306**, 809 (1988).
[69] M. Wakamatsu and H. Yoshiki, Nucl. Phys. **A524**, 561 (1991).
[70] C. V. Christov, A. Blotz, H.-C. Kim, P. Pobylitsa, T. Watabe, T. Meissner, E. Ruiz Arriola, and K. Goeke, Prog. Part. Nucl. Phys. **37**, 91 (1996).
[71] E. Witten, Nucl. Phys. **B160**, 57 (1979).
[72] E. Witten, Nucl. Phys. **B223**, 433 (1983).
[73] H.-C. Kim, A. Blotz, M. V. Polyakov, and K. Goeke, Phys. Rev. D **53**, 4013 (1996).
[74] H.-C. Kim, M. V. Polyakov, A. Blotz, and K. Goeke, Nucl. Phys. **A598**, 379 (1996).
[75] M. Wakamatsu and N. Kaya, Prog. Theor. Phys. **95**, 767 (1996).
[76] H.-C. Kim, M. Praszalowicz, and K. Goeke, Phys. Rev. D **57**, 2859 (1998).
[77] A. Silva, D. Urbano, and H.-C. Kim, Prog. Theor. Exp. Phys. **2018**, 023D01 (2018).
[78] J.-Y. Kim and H.-C. Kim, Eur. Phys. J. C **80**, 1087 (2020).
[79] J.-Y. Kim and H.-C. Kim, Eur. Phys. J. C **79**, 570 (2019).
[80] A. Silva, H.-C. Kim, D. Urbano, and K. Goeke, Phys. Rev. D **72**, 094011 (2005).
[81] Y.-S. Jun, J.-M. Suh, and H.-C. Kim, Phys. Rev. D **102**, 054011 (2020).
[82] J.-M. Suh, Y.-S. Jun, and H.-C. Kim, Phys. Rev. D **105**, 114040 (2022).
[83] H.-C. Kim, M. V. Polyakov, and K. Goeke, Phys. Rev. D **53**, R4715 (1996).
[84] H.-C. Kim, M. V. Polyakov, and K. Goeke, Phys. Lett. B **387**, 577 (1996).
[85] K. Goeke, J. Grabis, J. Ossmann, M. V. Polyakov, P. Schweitzer, A. Silva, and D. Urbano, Phys. Rev. D **75**, 094021 (2007).
[86] K. Goeke, J. Grabis, J. Ossmann, P. Schweitzer, A. Silva, and D. Urbano, Phys. Rev. C **75**, 055207 (2007).
[87] M. Wakamatsu, Phys. Lett. B **648**, 181 (2007).
[88] J.-Y. Kim, H.-C. Kim, M. V. Polyakov, and H.-D. Son, Phys. Rev. D **103**, 014015 (2021).
[89] P. V. Pobylitsa and M. V. Polyakov, Phys. Lett. B **389**, 350 (1996).
[90] P. Schweitzer, D. Urbano, M. V. Polyakov, C. Weiss, P. V. Pobylitsa, and K. Goeke, Phys. Rev. D **64**, 034013 (2001).
[91] D. Diakonov, V. Petrov, P. Pobylitsa, M. V. Polyakov, and C. Weiss, Nucl. Phys. **B480**, 341 (1996).
[92] D. Diakonov, V. Y. Petrov, P. V. Pobylitsa, M. V. Polyakov, and C. Weiss, Phys. Rev. D **56**, 4069 (1997).
[93] M. Wakamatsu and T. Kubota, Phys. Rev. D **57**, 5755 (1998).
[94] H.-D. Son, A. Tandogan, and M. V. Polyakov, Phys. Lett. B **808**, 135665 (2020).
[95] H.-D. Son, arXiv:2203.17169.
[96] J.-Y. Kim, H.-C. Kim, and M. V. Polyakov, J. High Energy Phys. 11 (2021) 039.
[97] H.-D. Son and H.-C. Kim, arXiv:2208.10150.
[98] G.-S. Yang, H.-C. Kim, M. V. Polyakov, and M. Praszałowicz, Phys. Rev. D **94**, 071502 (2016).
[99] H.-C. Kim, J. Korean Phys. Soc. **73**, 165 (2018).
[100] J.-Y. Kim, H.-C. Kim, and G.-S. Yang, Phys. Rev. D **98**, 054004 (2018).
[101] G.-S. Yang and H.-C. Kim, Phys. Lett. B **781**, 601 (2018).
[102] J.-Y. Kim and H.-C. Kim, Phys. Rev. D **97**, 114009 (2018).
[103] J.-Y. Kim and H.-C. Kim, Prog. Theor. Exp. Phys. **2020**, 043D03 (2020).
[104] G.-S. Yang and H.-C. Kim, Phys. Lett. B **801**, 135142 (2020).
[105] G.-S. Yang and H.-C. Kim, Phys. Lett. B **808**, 135619 (2020).

[106] J.-Y. Kim, H.-C. Kim, G.-S. Yang, and M. Oka, Phys. Rev. D **103**, 074025 (2021).
[107] D. Diakonov and V. Y. Petrov, Nucl. Phys. **B272**, 457 (1986).
[108] D. Diakonov, Prog. Part. Nucl. Phys. **51**, 173 (2003).
[109] F. Belinfante, Physica (Amsterdam) **6**, 887 (1939).
[110] W. Pauli and F. J. Belinfante, Physica (Amsterdam) **7**, 177 (1940).
[111] C. G. Callan, Jr., S. R. Coleman, and R. Jackiw, Ann. Phys. (N.Y.) **59**, 42 (1970).
[112] L. E. Parker and D. Toms, *Quantum Field Theory in Curved Spacetime: Quantized Field and Gravity*, Cambridge Monographs on Mathematical Physics (Cambridge University Press, Cambridge, England, 2009).
[113] M. V. Polyakov and P. Schweitzer, Int. J. Mod. Phys. A **33**, 1830025 (2018).
[114] C. Lorcé, P. Schweitzer, and K. Tezgin, Phys. Rev. D **106**, 014012 (2022).
[115] C. Lorcé, Eur. Phys. J. C **78**, 785 (2018).
[116] C. Lorcé, Phys. Rev. Lett. **125**, 232002 (2020).
[117] C. Lorcé and P. Wang, Phys. Rev. D **105**, 096032 (2022).
[118] M. V. Polyakov and P. Schweitzer, Proc. Sci., SPIN2018 (**2019**) 066 [arXiv:1812.06143].
[119] J.-Y. Kim and B.-D. Sun, Eur. Phys. J. C **81**, 85 (2021).
[120] C. Lorcé, L. Mantovani, and B. Pasquini, Phys. Lett. B **776**, 38 (2018).
[121] P. Schweitzer and K. Tezgin, Phys. Lett. B **796**, 47 (2019).
[122] I. A. Perevalova, M. V. Polyakov, and P. Schweitzer, Phys. Rev. D **94**, 054024 (2016).
[123] Y. Chen and C. Lorcé, arXiv:2210.02908.
[124] B. L. Ioffe, Nucl. Phys. **B188**, 317 (1981); **B191**, 591(E) (1981).
[125] K. Goeke, J. Ossmann, P. Schweitzer, and A. Silva, Eur. Phys. J. A **27**, 77 (2006).
[126] P. V. Pobylitsa, E. Ruiz Arriola, T. Meissner, F. Grummer, K. Goeke, and W. Broniowski, J. Phys. G **18**, 1455 (1992).
[127] A. Blotz, D. Diakonov, K. Goeke, N. W. Park, V. Petrov, and P. V. Pobylitsa, Nucl. Phys. **A555**, 765 (1993).
[128] J.-M. Suh, J.-Y. Kim, G.-S. Yang, and H.-C. Kim, Phys. Rev. D **106**, 054032 (2022).
[129] J. Ossmann, Angular momentum structure of the nucleon in the chiral quark soliton model, Ph.D. thesis, Ruhr-Universität, Bochum (main), 2005.
[130] C. Cebulla, K. Goeke, J. Ossmann, and P. Schweitzer, Nucl. Phys. **A794**, 87 (2007).
[131] J. Ossmann, M. V. Polyakov, P. Schweitzer, D. Urbano, and K. Goeke, Phys. Rev. D **71**, 034011 (2005).